

Feasibility of Natural Fibre Usage for Wind Turbine Blade Components: A Structural and Environmental Assessment – Supplementary Material

1 WTB description

Table S1 Additional WTB data

Blade scenario	All blade scenarios
Rated power (MW)	15
Blade length (m)	122.2
Root diameter (m)	6.4
Root cylinder length (m)	6.1
Cut-in wind speed (m/s)	3
Rated wind speed (m/s)	10.6
Cut-out wind speed (m/s)	25

2 ATOM design variables

Table S2: List of design variables (PS: pressure side, SS: suction side)

Name	#DVs	Normalised location of spline control points along the blade arc-length. 0:Root, 1: Tip	Comments
Shell UD	10	[0 0.02 0.05 0.1 0.25 0.4 0.6 0.8 0.9 0.95]	Baseline: glass
Shell Biax	10	[0 0.02 0.05 0.1 0.25 0.4 0.6 0.8 0.9 0.95]	Baseline: glass
Spar UDc (PS)	8	[0.05 0.1 0.25 0.4 0.6 0.8 0.9 0.95]	Baseline: carbon
Spar UDc (SS)	8	[0.05 0.1 0.25 0.4 0.6 0.8 0.9 0.95]	Baseline: carbon
Spar UDg	8	[0.05 0.1 0.25 0.4 0.6 0.8 0.9 0.95]	Baseline: glass
Web Biax	8	[0.04 0.1 0.25 0.4 0.6 0.8 0.9 0.96]	Baseline: glass
Web core	8	[0.04 0.1 0.25 0.4 0.6 0.8 0.9 0.96]	Baseline: foam
LE UD	5	[0.1 0.25 0.4 0.6 0.8]	Baseline: glass
LE core	7	[0.1 0.25 0.4 0.6 0.8 0.9 0.95]	Baseline: foam
TE UD	5	[0.1 0.25 0.4 0.6 0.8]	Baseline: glass
TE core	7	[0.1 0.25 0.4 0.6 0.8 0.9 0.95]	Baseline: foam

3 WTB manufacturing consumables model

Given the considerable quantities of consumables used during blade production, the impact of using these materials was included in the assessment. This required the development of a consumables model to estimate the quantity of consumables used with respect to the blade geometry. Developing the model in this way allows for rapid estimation of consumables used for a range of different blade structures and geometries. The mass of consumables used was estimated, for the most part, using the model outlined by the US National Renewable Energy Laboratory (NREL) in [1].

3.1 Vacuum bagging

The mass of bagging is proportional to the surface areas of the substructures and the area weight of the bagging material. Waste mass is given as a fraction of total mass required.

Equation S1: Total mass of bagging required

$$Mass_{bagging} = Area\ weight_{bagging} (Area_{webs} + Area_{HP\ mould} + Area_{LP\ mould} + Area_{spar\ caps} + Area_{Root}) + Waste$$

3.2 Peel-ply

The mass of peel-ply is proportional to the surface areas of the substructures and the area weight of the peel-ply fabric. Waste mass is given as a fraction of total mass required.

Equation S2: Total mass of peel-ply required

$$Mass_{peel-ply} = Area\ weight_{peel-ply} (Area_{webs} + Area_{HP\ mould} + Area_{LP\ mould} + Area_{spar\ caps} + Area_{Root}) + Waste$$

3.3 Tackifier adhesive

Tackifier adhesive is used in small amounts to adhere layers of layup materials / consumables during the layup process, so that they do not move relative to each other. The mass is estimated proportional to the mould areas, which are the sum of the areas of the moulds of webs, spar caps, root preforms, and main shells. Waste mass is given as a fraction of total mass required.

Equation S3: Total mass of tackifier adhesive required

$$Mass_{Tackifier\ adhesive} = Density_{Tackifier\ adhesive} \times Volume\ per\ area_{Tackifier\ adhesive} (Area_{webs} + Area_{spar\ caps} + Area_{root} + Area_{LP\ mould} + Area_{HP\ mould}) + Waste$$

3.4 Release agent

The mass of release agent is proportional to the mould areas and the volume of release agent per mould area used. Volume per area is provided in [1]. Waste mass is given as a fraction of total mass required.

Equation S4: Total mass of release agent required

$$Mass_{Release\ agent} = Density_{Release\ agent} \times Volume\ per\ area_{Release\ agent} (Area_{webs} + Area_{spar\ caps} + Area_{root} + Area_{LP\ mould} + Area_{HP\ mould}) + Waste$$

3.5 Flow medium

The mass of flow medium is proportional to the surface areas of the substructures and the area weight of the flow medium material. Flow medium coverage is given as the flow medium area relative to the substructure surface area and is given in [1]. When the spar caps are produced using prepregs, no flow medium is used for their production. Waste mass is given as a fraction of total mass required.

Equation S5: Total mass of flow medium required

$$Mass_{Flow\ medium} = Coverage \times Area\ weight_{Flow\ medium} (Area_{webs} + Area_{spar\ caps} + Area_{root} + Area_{LP\ mould} + Area_{HP\ mould}) + Waste$$

3.6 Tubing

This model assumes the use of tubes for both vacuum and resin feed lines. The mass of tubing is estimated as proportional to blade length, with model assumptions coming from [1]. Total mass of tubing per blade is given by:

Equation S6: Total mass of tubing per blade

$$Mass_{Tubing} = Linear\ weight_{Tubing} \times Length\ per\ blade\ length_{Tubing} \times Blade\ length + Waste$$

With eight substructures (2x shell, 2x spar cap, 2x shear web and 2x root prefab), the tubing used for each substructure is:

Equation S7: Mass of tubing using per substructure

$$Mass_{Tubing}(per\ substructure) = \frac{Mass_{Tubing}}{no.\ of\ substructures} = \frac{Mass_{Tubing}}{8}$$

Waste mass is given as a fraction of total mass required.

3.7 Tacking tape

The mass of tacking tape is assumed proportional to the blade length and the linear weight of the tacking tape, using assumptions made in [1]. Total mass of tacking tape per blade:

Equation S8: Total mass of tacking tape per blade

$Mass_{Tacking\ tape} = Length\ per\ blade\ length_{Tacking\ tape} \times Linear\ weight_{Tacking\ tape} \times Blade\ length + Waste$
Mass of tacking tape for a given substructure "X" is assumed to be proportional to the length of said component:

Equation S9: Mass of tacking tape for a given substructure

$$Mass_{Tacking\ tape-x} = Mass_{Tacking\ tape} \frac{Length_x}{\sum Length\ of\ all\ blade\ substructure}$$

Waste mass is given as a fraction of total mass required.

3.8 Masking tape

Masking tape is used to section off the area of the mould where tacking tape will be applied to for vacuum bagging. This is to protect the surface during mould release application so that the area of the mould that needs to have the tape applied does not become too slippery for tacking tape to adhere to. The length of

masking tape is therefore equal to the length of the tacking tape and the mass proportional to the length and the linear weight of the masking tape.

Total mass of masking tape per blade:

Equation S10: Total mass of masking tape per blade

$$Mass_{Masking\ tape} = Length\ per\ blade\ length_{Masking\ tape} \times Linear\ weight_{masking\ tape} \times Blade\ length + Waste$$

Mass of masking tape for a given substructure "X" is assumed to be proportional to the length of said component:

Equation S11: Mass of masking tape for a given substructure

$$Mass_{Masking\ tape-X} = Mass_{Masking\ tape} \frac{Length_X}{\sum Length\ of\ all\ blade\ substructure}$$

Waste mass is given as a fraction of total mass required.

3.9 Surface filler

Filler used to close small cracks and gaps on the blade surface prior to painting and its mass is assumed proportional to the blade outer area following assumptions made in [1].

Equation S12: The mass of surface filler required

$$Mass_{Filler} = Density_{Filler} \times Volume\ per\ blade\ surface\ area_{Filler} \times Blade\ surface\ area + Waste$$

Table S3 gives the assumptions and materials used in consumables models and mass of consumables used in blade production. Given the relevant blade geometries do not change across blade designs, the mass of consumables is constant across scenarios.

Table S3 Assumptions and materials used in consumables models and mass of consumables used. All waste estimates based on NREL blade cost model.

Consumable	Material	Assumption(s)*
Vacuum bagging	Nylon	Waste = 15% Area weight = 0.0525 kg/m ²
Peel-ply	Nylon fabric coated with 10% PTFE	Waste = 15% Area weight = 0.085 kg/m ²
Tackifier adhesive	PVA adhesive	Waste = 5% Density = 1190 kg/m ³ Volume per (mould) area = 3.06*10 ⁻⁵ m ³ /m ² [1]
Release agent		Waste = 5% Density = 792 kg/m ³ Volume per (mould) area = 2.57*10 ⁻⁵ m ³ /m ² [1]
Flow medium	Polypropylene	Waste = 15% Coverage = 70% [1] Area weight = 0.088 kg/m ²
Tubing	Nitrile rubber	Waste = 10% Length per blade length = 5 m/m [1] Linear weight = 0.4551 kg/m
Tacking tape		Waste = 5% Length per blade length = 10 m/m [1]

		Linear weight = 0.0633 kg/m
Masking tape	Paper and acrylic-based adhesive	Waste = 10% Length per blade length = 10 m/m (Assumed same as tacking tape [1]) Linear weight = 0.0076 kg/m
Surface filler	2-component PUR adhesive based on polyether and castor oil	Waste = 10% Volume per blade surface area = 0.0000204 m ² /m ³ [1] Filler density = 1330 kg/m ³

Table S4 Mass of consumables used in all blade scenarios.

	Mass (kg/WTB)
Bagging	106
Peel ply	172
Tackifier adhesive	67
Release agent	39
Flow medium	124
Tubing	611
Tacking tape	77
Masking tape	10
Surface filler	38

4 WTB manufacturing waste disposal

During blade production, waste is generated both from the blade materials and consumables used during production. This includes materials generated during infusion (i.e. excess resin in infusion tubing, vacuum bagging materials) and during trimming (i.e. flash trimming, fabric trimming). The waste quantity model for consumable materials was informed by assumptions made in [1] whereas the model for blade materials was informed by discussion with wind turbine OEM.

Table S5 gives the mass of waste materials generated and the mass of material disposed during blade production and the assumption used in waste model. In this context “Mass wasted” is the mass of a given material / consumable that has not been used in the production of the blade directly, but none the less, has been consumed during a given process (e.g. vacuum bagging trimming that is not actually used during infusion). “Mass disposed” is the total mass of the material / consumable that must be disposed of during production phase.

For consumables, this is generally the mass of the consumables used in the production in addition to the “mass wasted”. In the case of “tackifier adhesive” and “surface filler”, the used consumable is not disposed of, and becomes incorporated with the blade itself, therefore disposal mass is simply the same as the waste mass. Excess “release agent” is assumed to evaporate over time and not require disposal whether it is used or is wasted. For blade materials, the mass wasted simply equals the mass disposed (since blade material disposal is accounted for at end-of-life phase).

Table S5 Assumption used in blade production waste model.

Material	Production stage	Waste quantity model
Glass fibre	Fabric trim, flash trim	15% of BoM
Carbon fibre	Fabric trim, flash trim	15% of BoM
Basalt fibre	Fabric trim, flash trim	15% of BoM
Flax fibre	Fabric, flash trim	15% of BoM
Hemp fibre	Fabric, flash trim	15% of BoM
Resin	Infusion, flash trim	15% of BoM
Gel coat, top coat, primer	Coating spray up	10% of BoM
Core	Core trim	15% of BoM
Root attachments (steel)	N/A	0% of BoM
Lighting protection system (Aluminium)	N/A	0% of BoM
Vacuum bagging	Infusion / prepreg layup	15% of required mass
Peel-ply	Infusion / prepreg layup	15% of required mass
Tackifier adhesive	Infusion layup	5% of required mass
Release agent	Infusion / prepreg layup	5% of required mass
Flow medium	Infusion layup	15% of required mass
Tubing	Infusion / prepreg layup	10% of required mass
Tacking tape	Infusion / prepreg layup	5% of required mass
Masking tape	Infusion / prepreg layup	10% of required mass
Surface filler	Surface finishing	10% of required mass

Table S6 and Table S7 give the mass of consumables and blade structural waste disposed of during blade manufacturing. The mass of waste consumables is constant across the scenarios.

Table S6 Mass of consumables waste materials in all blade scenarios

	Mass (kg/WTB)
Bagging	106
Peel ply	172
Tackifier adhesive	3.2
Release agent	3.8
Flow medium	124
Tubing	611
Tacking tape	77
Masking tape	10
Surface filler	3.4

Table S7 Mass of blade structural material waste across the scenarios

Blade scenario	Mass (kg/blade)								
	Glass fibre	Carbon fibre	Flax fibre	Hemp fibre	Basalt fibre	Laminate resin	Core	Adhesive	Surface coating
Baseline (1)	5062	1361	0	0	0	2547	870	281	78
Flax (2.2)	3029	1325	1493	1493	1493	2120	892	271	78
Hemp (3.2)	3010	1300	1492	1492	1492	2098	883	269	78
Basalt (4.2)	3010	1300	1492	1492	1492	2098	883	269	78

5 WTB manufacturing approach

A high-level process flow of the entire blade manufacturing process used in the baseline impact assessment is presented in Figure S1. Offline prefabrication of blade sub-structures: shear webs, spar caps and root sections are assumed to take place prior to integration with the shell. VARTM is the most common method for producing the blade shells, with separate half shell infusion being used in the assessment. Blade manufacturing is then completed with assembly and finishing processes.

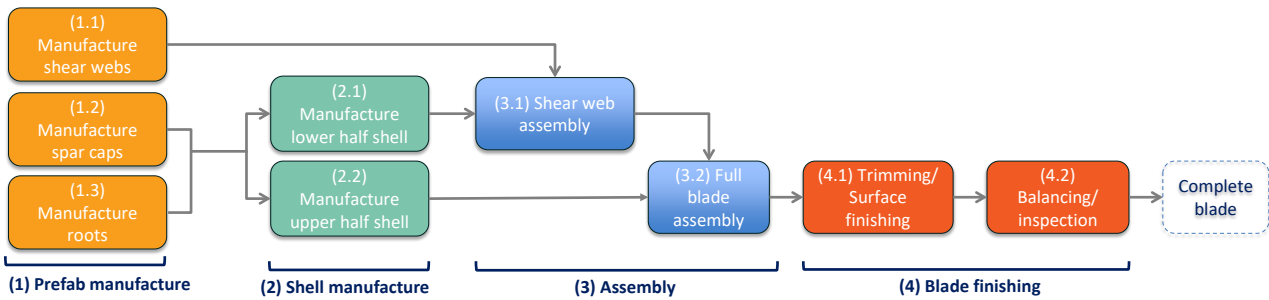


Figure S1 A high-level process flow of the entire blade manufacturing process used in the baseline impact assessment

Table S8 High-level description of blade manufacturing stages and processes

Manufacturing stage	Process description
(1.1) Shear web / (1.3) Root prefabrication	VARTM alone is selected for baselines assessment.
(1.2) Shear web prefabrication	Three manufacturing processes: VARTM, prepreg and pultrusion, are selected for the baselines assessment.
(2.1) / (2.2) Shell production	Prefabricated spar cap and root sections are inserted into the shell mould as part of the layup prior to shell infusion. While consolidation through adhesive bonding, following shell curing, has been identified this does not appear to be currently used widely.
(3.1) Shear web assembly	Following blade curing, the shear webs are bonded to the spar cap, within the lower shell inner surface, using adhesive.
(3.2) Full blade assembly	Carried out by simultaneously bonding the shear webs to the upper shell, and bonding the upper and lower shell perimeters (this is achieved using “clam shell” style closed moulds). Thermal post curing of the whole blade structure is carried out using heated tooling, followed by demoulding after cooling.
(4.1) Trimming/surface finishing	The assembled blade is lifted onto a transport cart and moved to the finishing area, where flash trimming, surface finishing, painting and root machining is conducted.
(4.2) Balancing/inspection	Finally, the blade is balanced and inspected prior to transportation to onsite location.

6 WTB manufacturing energy models

6.1 Resin infusion

Energy demand for the resin infusion stages was informed by primary data obtained by NCC during a large-scale vacuum infusion trial. The total energy demand for the resin infusion step was assumed to be proportional to the mass of the resin infused which was measured to be 0.91 MJ/kg resin. The energy demand required to infuse a given blade is given below:

Equation S13: The energy demand required to infuse a given

$$Energy_{infusion} = 0.91 \times Resin\ mass$$

Table S9 gives the resin mass and energy of infusion across the scenarios.

Table S9 Resin mass and energy of infusion across the blade scenarios

Blade scenario	Resin mass infused (kg)	Infusion energy demand (MJ)
Baseline (1)	19524	17727
Flax (2.2)	21154	19208
Hemp (3.2)	20957	19029
Basalt (4.2)	20957	19029

6.2 Flash trimming

Flash trimming involves cutting the excess fibre/resin present at the perimeter of the part. This is conducted following demoulding the shear webs, spear caps and root prefabs. The flash is trimmed from the blade shells following bonding upper and lower shell halves. Trimming is assumed to be conducted using a handheld circular saw with a max. rated power of 750 W. Trim rate by a single circular saw was assumed to be 10 m/hr in line with the methodology outlined in [1]. Energy demand from flash trimming for a given substructure is a function of the time to trim and the max. rated power of the circular saw and is given as:

Equation S14: Energy demand from flash trimming for a given substructure

$$Energy_{flash\ trim} = \frac{Trim\ length\ [m]}{Trim\ rate\ [\frac{m}{s}]} \times Circular\ saw\ max.\ power\ [W]$$

Where trim length is the part/mould perimeter and is assumed to be twice the part length gives the trim lengths, cycle times and energy associated with flash trimming for each blade scenario. Note, the cycle time is the total time to trim each part but can be conducted concurrently by multiple personnel. Given the trim length does not change between blade designs, the energy demand is the same across scenarios.

Table S10 Trim lengths, cycle time and energy associated with flash trimming for all blade scenarios.

Total trim length (m/blade)	1248
Cycle time (hr/blade)	125
Total energy demand (MJ/blade)	337

6.3 Adhesive

Adhesives are commonly applied with two-component metering and mixing equipment. The resin and the hardener are mechanically pumped or extruded from their containers, through delivery pipes, to the mixer head where the two components are thoroughly blended and discharged. Energy to apply adhesive was estimated based on the max. power consumption (26 kW) of a “Twin Engineers - Adhesive mixing machine” and estimated cycle time for applying adhesive. Cycle time estimates were based on max. adhesive mass flow rate (20 kg/min) and the mass of adhesive required for each stage. Energy associated with adhesive application was therefore given by:

Equation S15: Energy demand associated with adhesive application

$$Energy_{adhesive\ app.} = \frac{Adhesive\ mass [kg]}{Adhesive\ flow\ rate [kg/s]} \times Adhesive\ machine\ max.\ power [W]$$

Table S11 Adhesive mass and energy demand for all blade scenarios.

Adhesive mass [incl. waste] (kg)	Energy demand (MJ)
3744	292

6.4 Warehouse transportation

Blade structure and substructures were assumed to be transportation throughout the manufacturing facility using electric warehouse transportation carts. The power consumption of the electric carts, along with the cycle/transportation time to move the component, was used to estimate the energy associated with moving the blade/substructures. The max. power of the cart is assumed to be dependent on the carry capacity with the following two carts used depending on the mass of the component being transported:

- Cart A: AICRANE AQ-KPJ-20T – up to 20 tonne – max. power consumption = 2.5 kW
- Cart B: AICRANE AQ-KPJ-150T – up to 150 tonne – max. power consumption = 15 kW

The energy demand associated with transportation of a given blade structure within the warehouse is given as follows:

Equation S16: Energy demand associated with transportation of a given blade structure within the warehouse

$$Energy_{warehouse\ transport} = Cycle\ (transport)\ time \times max.\ power\ of\ cart$$

The cycle (transportation) time is found using the methodology outlined in [1]; "Megawatt-size blades require a minimum of 10 minutes to be moved, with a premium of 1/3 minute per extra meter of blade length above 60 m due to extra complexity with larger blade lengths". The blade production requires the transportation of large blade substructures (i.e spar cap and shear web), the same methodology to calculate cycle (transportation) time was used for these parts, as is outline by [1] for full blade structure.

Table S12 Cycle time, cart type used and energy demand associated with component transportation within warehouse.

Cart A cycle time (min/blade)	Cart B cycle time (min/blade)	Total energy (MJ/blade)
130	123	130

6.5 Warehouse lifting

It is assumed that overhead cranes are used to lift the blade and blade substructures during manufacturing within the warehouse. This occurs during part demoulding, transferring to warehouse transportation carts as well as placement of substructures such as spar caps, shear webs and root prefabs within the blade shell. The power consumption of the crane, along with the cycle time to lift the component, was used to estimate the energy associated with lifting the blade/substructures. The max. power of the crane is assumed to be dependent on the carrying capacity with the following two cranes used depending on the mass of the component being transported:

- Crane A: AICRANE AQ-LH – up to 10 tonne – max. power consumption = 39.5 kW
- Crane B: LIEBHERR LTM 1100-4.2– up to 100 tone – max. power consumption = 129 kW

The energy demand associated with lifting a given blade structure within the warehouse is given as follows:

Equation S17: Energy demand associated with lifting a given blade structure within the warehouse

$$Energy_{warehouse\ lifting} = 50\% \text{ Cycle time} \times \text{max. power of crane}$$

The cycle time to lift / insert prefabricated blade substructures, as well to demould the entire blade, have been estimated in [1] and are described in Table S13. It is assumed that the crane will not require energy input during the whole lifting cycle time, a nominal knock down of 50% is use – i.e. it is assumed the crane demands power for half the lifting time. The impact of this assumption is assessed in the sensitivity analysis.

Table S13 Cycle time assumptions and crane type to lift, demould and insert the various structures

Manufacturing stage	Description / source	Crane type
Insert root prefab	"...it is assumed to take 15 minutes" [1]	Crane A
Insert spar cap (Upper/Lower)	"workers can insert a 30-meter-long (or less) spar cap in 15 minutes, with an additional premium of 5 minutes per extra 10 m of spar cap length above 30 meters" [1]	Crane A
Insert shear web (1/2)	Assumed using same method as used for spar cap insertion.	Crane A
Insert upper shell		Crane B
Full blade demould and transfer to cart	"All megawatt-size blades and above require a minimum of 15 minutes to be transferred to carts. However, because of extra complexity with larger blade lengths, a premium of 1 minute per extra meter of blade length above 60 m should be added.	Crane B
Demould root prefab	Assumed the same cycle time as inserting into shell	Crane A
Demould spar cap (Upper/Lower)		Crane A
Demould shear web (1/2)		Crane A

Table S14 Cycle time and energy demand to lift, demould and insert the various structures for all blade scenarios

Crane A cycle time (min/blade)	Crane B cycle time (min/blade)	Total energy (MJ/blade)
529	138	1163

6.6 Blade surface sanding

Surface sanding involves sanding the blade surface following surface filling in preparation for surface coating application. Sanding is assumed to be conducted using a handheld orbital sander with a max. rated power of 280 W. Sanding rate by a single orbital sander was assumed to be 6 m²/hr in line with the methodology outlined in [1]. Energy demand from sanding for a given substructure is a function of the time to sand and the max. rated power of the orbital sander and is given as:

Equation S18: Energy demand from sanding for a given substructure

$$Energy_{sanding} = \frac{Blade\ surface\ area [m^2]}{Sanding\ rate [m^2/s]} \times Sander\ max.\ power [W]$$

Where blade surface area is the sum of the high and low pressure shell outer surface area gives the sanding area, cycle time and energy demand during blade surface sanding. Note, the cycle time is the total time to sand the blade but can be conducted concurrently by multiple personnel. Given the blade surface area does not change between blade designs, the energy demand is constant across the scenarios.

Table S15 Sanding area, cycle time and energy demand during blade surface sanding

Sanding area (m ² /blade)	Cycle time (hr/blade)	Energy demand (MJ/blade)
1262	210	212

6.7 Surface coating

Surface coating are assumed to include gel coat, primer and top coat. Gel coat is applied directly onto the shell moulds prior to lay up and lamination. Primer and top coat are applied to the blade surface following sanding. In all cases it is assumed the coatings are applied via compressed air spray guns. These equipment use an electric compressor which is the source of energy demand during these processes. Power consumption of such equipment was based on an industrial spray gun / compressor system which a max. power consumption of 2.2 kW. Spray rate for a single spray gun was assumed to be 120 m²/hr based on the methodology outlined in [1]. Energy demand from surface coatings application for a given substructure in given as:

Equation S19: Energy demand from surface coatings application for a given substructure

$$Energy_{coating\ application} = \frac{Part\ surface\ area [m^2]}{Spray\ rate [m^2/s]} \times Spray\ gun/compressor\ max.\ power [W]$$

Table S16 gives the spray area, cycle time and energy demand during coatings application. Note, the cycle time is the total time to apply coatings but can be conducted concurrently by multiple personnel. Given the blade surface areas do not change between blade designs, the energy demand is constant across the scenarios.

Table S16 Spray area, cycle time and energy demand during coatings application

Blade scenario	Spray area (m2/blade)	Cycle time (hr/blade)	Energy demand (MJ/blade)
All blade scenarios	3786	32	250

6.8 Thermal post curing

The energy input required to conduct the thermal post curing treatment of the blade/blade substructures was modelled. Total energy input during the post curing is assumed equal to the sum of the energies required to bring the blade/blade substructures to temperature, the tooling to temperature and the total heat lost during the post curing schedule. This is given below as:

Equation S20: Energy input associated with part thermal post curing treatment

$$Q_{cure-total} = Q_{part} + Q_{tool} + Q_{loss}$$

energy input to bring the part to temperature (Q_{part}) is given as:

Equation S21: Energy input to bring the part to post cure temperature

$$Q_{part} = mass_{part} \times Cp_{part} \times (T_{cure} - T_{amb}) \times \eta_{heater}$$

Cp_{part} was found by weighted averaging the Cp of the constituent materials in the part. η_{heater} is the heater efficiency with a nominal value of 50% selected.

The average temperature across the composite tooling “equipment wall” was found to be approximate to that of the part curing temperature therefore the energy associated with heating this part of the tooling must be included in the energy input also. This requires the mass of the tooling to also be estimated.

Table S17 Cure schedule and energy required during thermal post curing for each of the blade scenarios.

Blade scenario	Cure temperature (°C)	Cure time (hr)	Energy demand (MJ)
Baseline (1)	60	15	17009
Flax (2.2)	60	15	17025
Hemp (3.2)	60	15	16908
Basalt (4.2)	60	15	16908

6.9 HVAC

The electricity and natural gas consumption required for the WTB manufacturing facility atmospheric control (using its HVAC system) was estimated based on assumptions and methodology described in [10]. Table S18 gives the estimated energy demand from facility atmospheric control (HVAC). * Workshop floor space estimated using methodology outlined in [1], assuming facility has capacity to produce 250 WTB annually. ** General office and Storage warehouse assumed to be 25% the floor space of the Workshop.

Table S18 Estimated energy demand from facility atmospheric control (HVAC)

	Electricity typical benchmark [kWh/m2]	Fossil-thermal typical benchmark [kWh/m2]	Surface area [m2]	Total electricity per blade [kWh]	Total thermal energy from NG per blade [kWh]
Workshop	35	180	16256*	2275.891557	11704.58515
General office	95	120	4064**	1544.354985	1950.764192
Storage warehouse	35	160	4064**	568.9728893	2601.018923
Total				4389.219432	16256.36827

7 WTB commissioning model

7.1 Blade installation

The WTs consist of different components, including blades, hub, nacelle, tower. Current practice in WT installation shows that different strategies have been devised by wind farm installation companies depending on the available vessels/equipment, port facilities, and safety considerations. Figure S2 shows the different installation methods for WTs alongside their required number of offshore lifts [11]. This report assumed Method 2 is used. In this method, the tower is assembled onshore and installed as a single part in a single lift. Then, the nacelle with a pre-attached rotor hub is mounted on the top of the tower. The installation operation is followed by three separate lifts for the blades. Thus, this method includes 5 independent lifts. It is assumed that a Jackup Vessel (JUV) is used to transport and lift the WT subsections. It is assumed that one JUV has cargo capacity of 8 total WT systems which it installs in series in a single trip at sea.

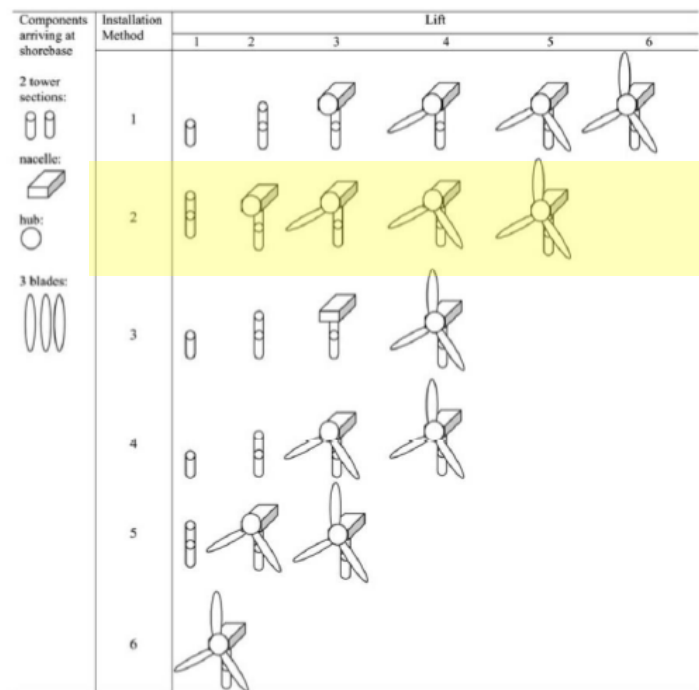


Figure S2 Different installation methods for WTs

Table S19 gives the estimated durations of the various offshore installation operations [2].

Table S19 Installation operation duration

Installation operation	Duration (hr)
JUV positioning time	3
JUV jack up time	6
Single blade installation	4
Nacelle installation	4
Tower installation	6
JUV jack down time	2
Total lift time per turbine	25

Fuel consumption of the JUV during the WT installation is estimated based on the total installation time of the WT and literature JUV fuel consumption data of 0.42 t/hr [12]. Fuel consumption of the JUV during transit is also calculated based on the known JUV transit distance during the entire trip (i.e., to install all 8 WT) (port-to-windfarm = 115 km, WT-to-WT = 1 km), known JUV transit speed of 10 knots [12], and fuel consumption of 0.42 t/hr [12]. Fuel consumption is converted into the impact indicators using emission factors taken from the GaBi model "Bulk commodity carrier, 5,000 to 200,000 dwt payload capacity, ocean going", in case of combustion of 1kg of heavy fuel oil (Table S20).

During installation operations, the JUV are lifting and transporting dissimilar structures, beyond just the WTB. The total fuel consumption of the JUV during the installation was calculated and fuel allocated to the WTB based on the time contribution of the blade installation activities to the total WT installation time. One blade installation is estimated be 17% of the total WT installation time, resulting in 2,306 kg of HFO consumed.

Table S20 Emissions factors in case of combustion of 1kg of heavy fuel oil

	Emission factors - combustion of 1kg of Heavy fuel oil (1.0 wt.% S) [Refinery products]
Carbon dioxide [Inorganic emissions to air]	3.114000000000000000
Carbon dioxide (biotic) [Inorganic emissions to air]	0.000000000000000000
Carbon monoxide [Inorganic emissions to air]	0.0027700000000000100
Dust (PM2.5) [Particles to air]	0.0072800000000000000
Methane [Organic emissions to air (group VOC)]	0.0000600000000000001
Nitrogen oxides [Inorganic emissions to air]	0.09030000000000001000
Nitrous oxide (laughing gas) [Inorganic emissions to air]	0.0001500000000000000
NMVOG (unspecified) [Group NMVOG to air]	0.0030800000000000000
Sulphur dioxide [Inorganic emissions to air]	0.0500000000000000000

8 Operation and maintenance model

Given the high transit distance from the coast (115 km), it is impractical for the turbine to be serviced by a port-based work boat. It is assumed the turbine will be serviced by an offshore-based vessel with accommodation for personnel which does not need to return to port daily [13]. Such vessels are termed SOVs (Service Operation Vessels) which are large vessels designed to be a platform for wind farm support, operating within the wind farm for weeks at a time. SOVs naturally have longer endurance periods and tend to operate on 14-21 day rotations before needing to return to port [14].

The impact of O&M was quantified by estimating the vessel fuel used during 1) regular scheduled inspections, 2) rail activities. SOV fuel consumption during regular WT inspections is given in [14]. It was assumed that the system wide inspection rate is 1.44 WT inspection per year [3]. Repair rates for various offshore wind turbine sub-systems was measured as part of the SPARTA program, which found an average of 0.115 repair trips per month per turbine explicitly for turbine rotor repair work [3]. It was assumed that four WTs can be inspected / repaired in parallel from a single SOV [14], with each WT requiring one or two days per inspection or repair respectively. The fuel consumption of the SOV during inspection / repair works was allocated evenly across all WT substructures being inspected (assuming 15 sub-structures per WT being inspected) / repaired. The SOV fuel consumption was considered for periods where vessel was in transit or idle on site, which each have different consumption rates as shown in Table S21.

Table S21 Fuel consumptions assumptions made in O&M model

Metric	Value	Unit
Fuel consumption in transit	1000 [14]	litres/hour
Fuel consumption in idle	120 [14]	litres/hour
Fraction of time spent in transit	52% [14]	
Fraction of time spent idle	48% [14]	

Fuel consumption is converted into the impact indicators using emission factors taken from the GaBi model in case of combustion of 1kg of light fuel oil Table S21. Total O&M fuel consumption across the WTB lifecycle was estimated to be 25,677 kg.

Table S22 Emissions factors in case of combustion of 1kg of heavy fuel oil

	Emission factors - combustion of 1kg of Light fuel oil (0.05 wt.% S) [Refinery products]
Carbon dioxide [Inorganic emissions to air]	3.151000000000100000
Carbon dioxide (biotic) [Inorganic emissions to air]	0.000000000000000000
Carbon monoxide [Inorganic emissions to air]	0.002770000000000000
Dust (PM2.5) [Particles to air]	0.0042600000000000100
Methane [Organic emissions to air (group VOC)]	0.0000600000000000001
Nitrogen oxides [Inorganic emissions to air]	0.09030000000000001000
Nitrous oxide (laughing gas) [Inorganic emissions to air]	0.0001500000000000000
NMVOG (unspecified) [Group NMVOG to air]	0.0030799999999999900
Sulphur dioxide [Inorganic emissions to air]	0.0010000000000000000

9 WTB decommissioning model

The WT decommissioning is assumed to be the reverse of the installation with the only difference being that, as the WT sub-structures (e.g., blades, hub, nacelle, tower) are removed using a JUV, they are loaded onto a barge vessel [2]. The barge vessel is then tugged (using a tugboat) back to port for unloading. Decommissioning activity times are given in Table S23. It is assumed that one barge vessel has the capacity to transport one full disassembled WT. The fuel consumption of the tugboat during transit is based on the known transit distance (port-to-windfarm = 115 km), known tugboat transit speed of 8 knots [15], and fuel consumption of 0.32 t/hr [16]. Fuel consumption is converted into the impact indicators using emission factors taken from the GaBi model in case of combustion of 1kg of light fuel oil (Table S22).

The total fuel consumption of the JUV during the decommissioning was calculated and fuel allocated to the WTB based on the time contribution of the blade decommissioning activities to the total WT decommissioning time. One blade installation is estimated to be 21% of the total WT installation time, resulting in 2,954 kg of fuel consumed.

Table S23 Decommissioning operation duration

Installation operation	Duration (hr)
JUV positioning time	3
JUV jack up time	6
Single blade removal	2
Nacelle removal	3
Tower removal	4
JUV jack down time	2
Total lift time per turbine	20

10 WTB EoL assumptions

10.1 Downsizing

It was assumed that some level of downsizing of the blade is required regardless of the EoL scenario. Two methods for downsizing are considered depending on the EoL scenario. It is assumed for all EoL scenarios that the blade is initially shredded. This is assumed to be carried out on the port site via a low speed, high torque shredder. Some recycling scenarios require secondary downsizing which is assumed to be conducted using a granulator.

10.1.1 Shredding

The energy demand required to conduct the shredding was estimated based on the energy demand provided by a supplier of industrial shredding equipment with data presented in Figure S3 for a range of shredder sizes. The energy demand was found assuming actual shredder power is equal to 60% of maximum rated power under conditions of maximum throughput, as suggested in communications with shredder supplier “Summit Solutions”. It is assumed that the shredding will be conducted using large scale equipment therefore the energy consumption will, at most, be that of the Zerma ZXS 3000 at 0.11 MJ/kg of FRP.

Equation S22: Shredder energy consumption

$$Energy_{shredder}[MJ] = 0.11 \times Mass_{blade}[kg]$$

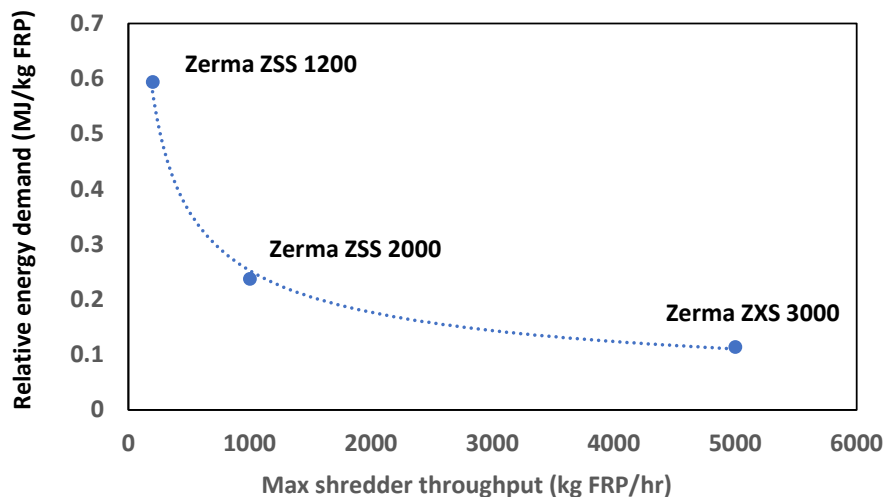


Figure S3 Maximum throughput and relative energy demand of a range of shredders with differing capacities as provided by Summit System

10.1.2 Granulation

It is assumed that energy consumption during granulation is 0.27 MJ/kg of blade waste based on granulator primary energy data reported in [7] when processing similar composite material.

10.2 Waste transport

The transportation from the coast to the landfill site has been modelled using the GaBi LCI secondary dataset “Articulated lorry transport incl. fuel, Euro 0-6 mix, 40 t total weight, 27 t max payload”. It is an aggregated LCI dataset that includes the LCI data about the fuel production used by the lorry (“well to tank” impact) and by the tailpipe emissions (“tank to wheel” impact).

The mass transported has been considered equal to the whole blade waste mass. The assumed transportation distances are given in Table S24. Waste by-products generated during the recycling EoL scenarios have assumed transportation distance to final waste disposal (either landfill or incineration) equal to 100 km.

Table S24 Assumed transportation distances for WTB waste

EoL scenario	Transportation distance (km)	Description
<ul style="list-style-type: none"> • Landfill • Incineration 	100	It is assumed that a landfill / EfW facility will be in close proximity regardless of location of waste.
<ul style="list-style-type: none"> • Cement kiln • Mechanical recycling • Pyrolysis recycling 	500	It is assumed that recycling facilities for EoL WTBs will be more sparsely distributed across the UK, therefore, nominally larger waste transportation distance has been selected.

10.3 Metallics

The following metallic components will be present in the decommissioning blade:

- Blade root attachment inserts (steel)
- Lightning protection system (aluminium)

Following blade shredding it is assumed these metallics will be recovered from the shredded blade waste and will be sent for recycling. It is believed that this is a reasonable assumption given the widespread recycling of steel and aluminium, and the financial opportunity for a blade recycler to resale metal scraps. The extraction and recycling of the metals is out with the scope of this LCA and therefore the impact associated with any processes to reclaim and recycling the metals has not been considered. In balance, no avoided burden has been attributed to the blade at EoL (as has been done for other recycled materials e.g. carbon / glass fibre). The metallic components therefore do not incur any impact at EoL, and as a consequence, no additional credit has been awarded to the blade despite being a source of valuable scrap metals.

10.4 Landfill

Table S25 Assumptions and datasets used for landfilling the various blade materials

Material	Assumption / landfill dataset
Glass fibre	A data set specifically for glass or basalt fibre landfilling was not available in the GaBi LCI dataset, therefore the “EU-28 - Inert matter (Glass) on landfill” dataset was used as a proxy, as it is assumed this will have similar impact given comparable composition and stability in landfilling.
Basalt fibre	
Carbon fibre	A data set specifically for carbon fibre landfilling was not available in the GaBi LCI dataset, therefore the “EU-28- Plastic waste on landfill” dataset was used as a proxy, as it is assumed this will have similar impact given comparable composition and stability in landfilling.
Flax fibre	A data set specifically for Balsa, flax fibre or hemp fibre landfilling was not available in the GaBi LCI dataset, therefore the “EU-28 - Untreated wood on landfill” dataset was used as a proxy, as it is assumed this will have similar impact given comparable composition and stability in landfilling.
Hemp fibre	
Epoxy	A data set for landfilling specific polymer types was not available in the GaBi LCI dataset, therefore the “EU-28 - Plastic waste on landfill” dataset was used for all polymers.
PET core	
Adhesive	
Surface coatings	

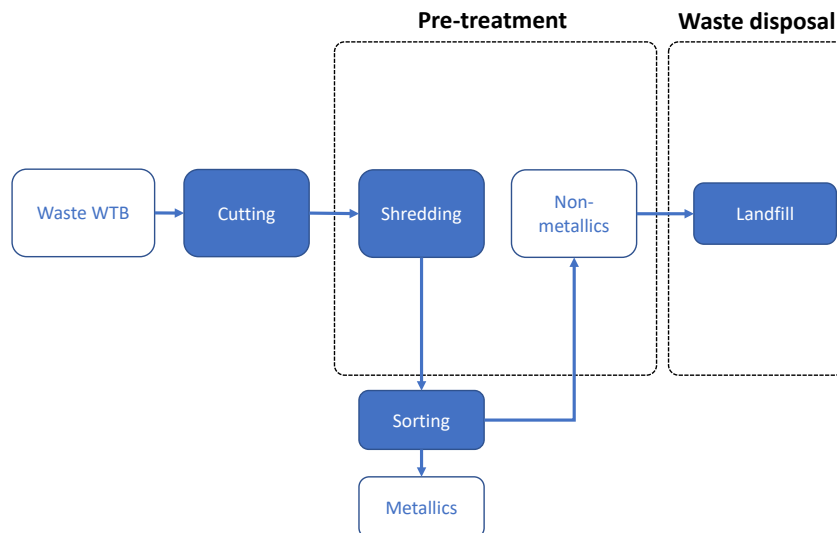


Figure S4 Process flow for WTB disposal in landfill

10.5 Energy from waste

Incineration of waste enables the chemical energy to be extracted which can be transformed into usable electrical power as well as heat energy in some cases. Wind blade waste can be co-processed with solid municipal waste within well-established Energy from Waste (EfW) facilities. While energy is recovered from

the waste, this process is unable to reclaim the non-combustible fractions and is therefore not considered to be a true recycling process. The energy produced depends on the waste energy content and the incineration plants efficiency at generating useful energy.

The calorific value of the waste is determined by the calorific value of the blade's constituent materials and their fraction in the waste feedstock. Table S29 gives the aggregated calorific value of wind blade waste from each of the scenarios assessed. EfW facilities vary in efficiency, with typical electrical efficiencies of 15-24% [17]. Plants operating in combined heat and power mode can increase the overall plant efficiency to over 70% by utilising waste heat which would otherwise be lost to the environment in the condenser [17]. Since the focus of this study is UK waste GRP solutions, the average efficiency across all UK energy from waste plants is used in the model.

As of 2019, only 10 out of 48 UK operational energy from waste plants utilise heat recovering, with the majority only generating electrical power [18]. The UK average electrical power and heat generated in 2019 was 531 kWh/t and 110 kWh/t respectively [18]. With an average feedstock calorific value of 9.2 MJ/kg [18], this gives overall electrical power and heat efficiencies of 20.7% and 4.3% respectively. Electricity generated is assumed to displace the UK mains electrical supply whereas heat is assumed to offset heat production from natural gas combustion, assuming 80% efficiency (generation of heat in fired boilers ranges from 50% to about 90% [19]).

While the bottom ash from energy from waste plants can be reused as filler products in the construction industry, it is unclear at what rate this occurs in practice and exactly what this material is displaced in the supply chain. It is therefore assumed that residual fraction of the blade waste is landfilled. Residual mass following incineration is equal to the mass of glass fibre input to the system, as it is assumed all other materials are fully oxidised and leave the system as gases.

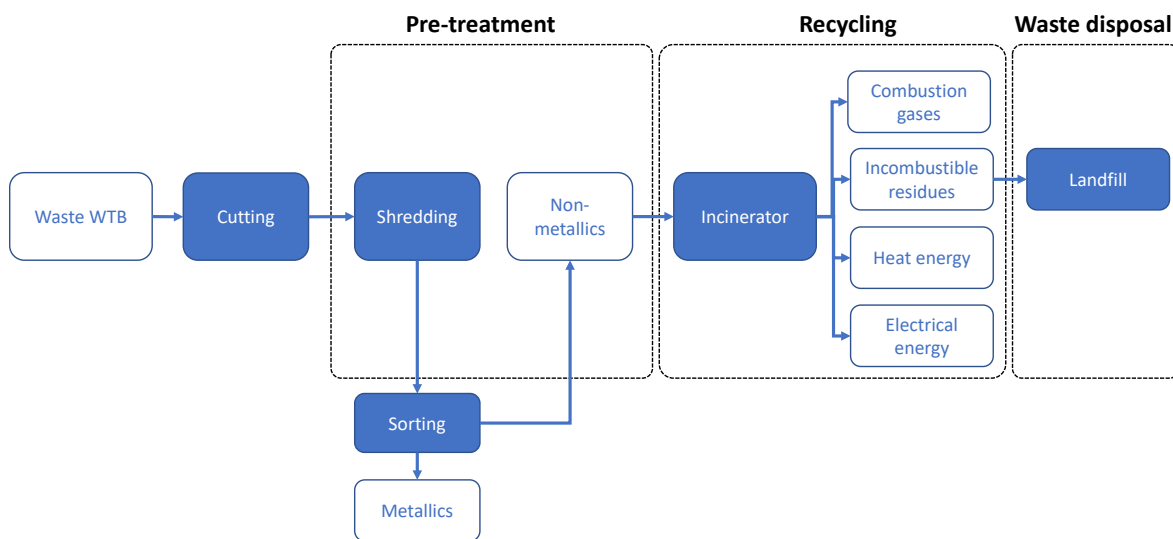


Figure S5 Process flow for WTB disposal using incineration with energy recovery.

10.6 Cement kiln co-processing

WTB waste is already commercially used as both fuel and raw materials in the production of clinker within cement kilns. The production process combines raw material fractions with an energy source (fossil fuel) and heated to around 1450 °C to produce cement clinker; composed of calcium oxide, silica, alumina and iron oxide. WTB waste is an idea raw material for cement manufacturing since “the mineral composition of glass fibre is consistent with the optimum ratio between calcium oxide, silica and alumina”[6]. Calcium carbonate

is a raw material in clinker production which is calcified to calcium oxide within the kiln; it is assumed this can be offset with the calcium oxide present in the glass fibre. Combustion of the organic fraction of the WTB waste within cement kilns can be used to heat the process and offset demand for petroleum coke. This route allows all the waste to be utilised and nothing is landfilled. In this study it is assumed that WTB waste can replace petroleum coke at an energy equivalence basis following Equation S23. This replacement rate is dependent on blade calorific value and varies between scenarios, for the baseline scenario the replacement rate was 0.36.

Equation S23: Petroleum coke replacement rate on cement kiln

$$\text{Replacement rate} = \frac{m_{\text{coke}}}{m_{\text{WTB}}} = \frac{CV_{\text{WTB}}}{CV_{\text{coke}}}$$

E-glass with silica, calcium oxide and alumina content of 54, 18 and 15 %wt. respectively was used in modelling the cement kiln co-processing route. It was assumed all minerals will directly replace raw materials on a mass equivalency basis, offsetting the energy and emissions associated with upstream production of these materials.

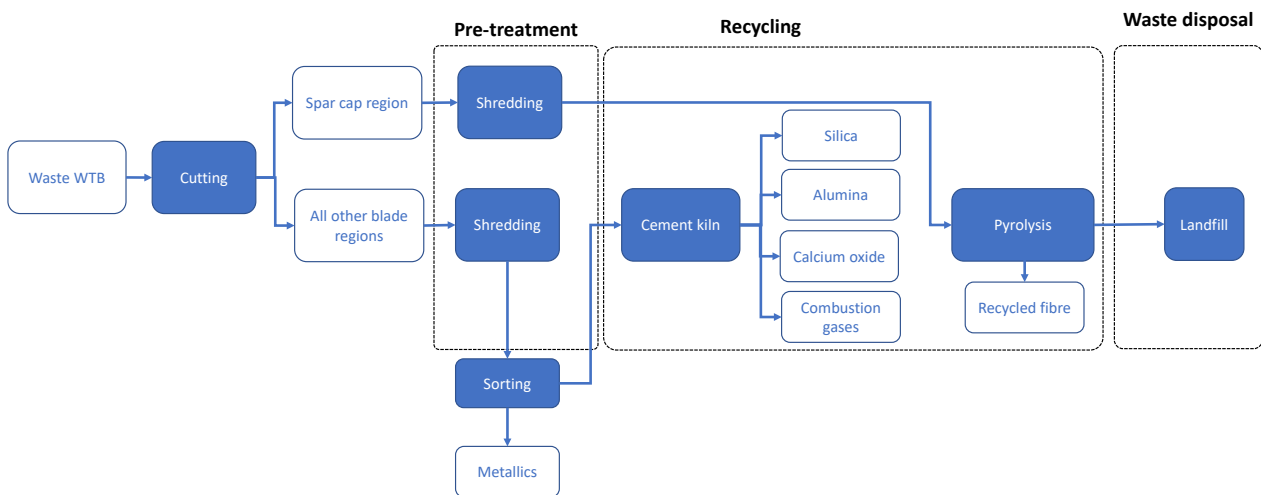


Figure S6 Process flow for WTB co-processing in cement kiln

10.7 Mechanical recycling

Mechanical recycling of WTB waste was modelled using a downsizing and classification process outlined in [4]. WTB waste is first ground using a granulator then classified into four fractions using a “zig-zag” classifier. The four distinct fractions differ in composition and size, with the process producing two fibre rich fractions, a “coarse” resin rich fraction and a final “powder” fraction. The coarse resin fraction is then reprocessed again (granulation and classification) to extract more fibrous materials. The resulting composition of the granulated and classified fractions are given in Table S26.

Table S26 Mechanical recycling fractions

	Fraction of waste	
	After 1x granulation + classification	After 2x granulation + classification
Fibrous fraction	42%	54%
Coarse resin rich fraction	28%	8%
Powder fraction	30%	38%

Energy demand for both downsizing and classification stages required for mechanical recycling were modelled. Downsizing energy using a granulator was calculated using the method outlined in [7]. Energy demand for “zig-zag” classification is highly dependent on equipment size, flow rates and particulate loading, which is modelled and measured experimentally in [20]. A nominal energy demand for classification of 5 kJ/kg GRP was selected based on an average of measured data in [20], which must be repeated to obtain the four GRP fractions. All energy for mechanical recycling is assumed to be electrical and sourced from UK mains supply.

It is assumed that the recovered fibre rich fractions can offset the production of virgin glass fibre, which would otherwise be used in the production of injection moulded products. No use has been fully demonstrated for the coarse and powder fractions. It is proposed that the powder fraction may be used as filler (such as in neat or reinforced polymer applications), and as a result, offset the production of powdered calcium carbonate filler material. In this study it is assumed that the filler fraction output can offset equal mass of calcium carbonate production. The coarse, resin rich fraction, is assumed to be a waste product in the study and is disposed of via landfill.

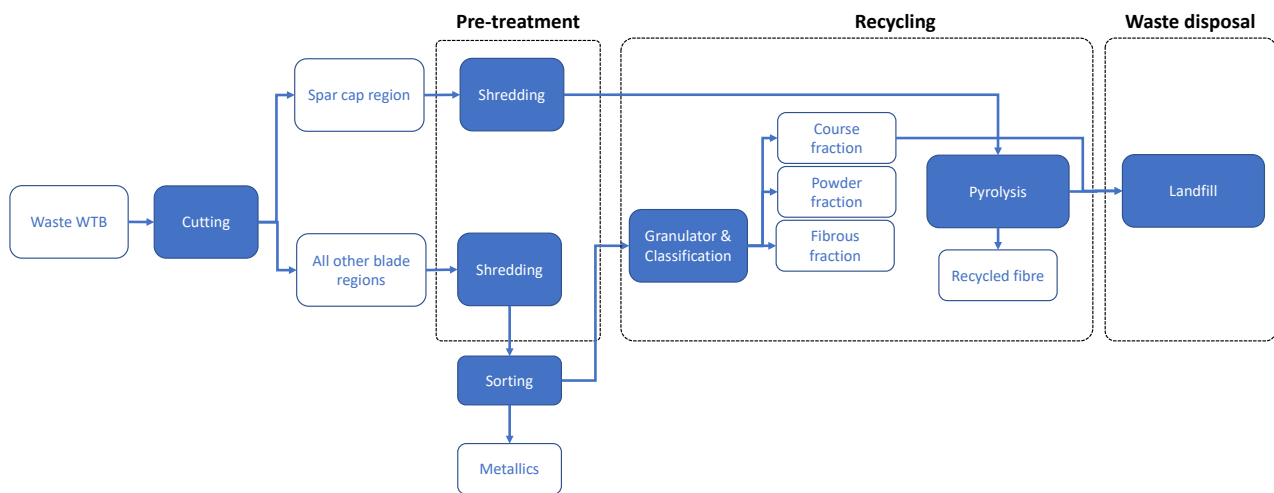


Figure S7 Process flow for WTB disposal using mechanical recycling.

10.8 Pyrolysis recycling

Thermal recycling of WTB waste using pyrolysis involves decomposition of polymers without (or in low) oxygen at high temperatures between 300 and 800 °C [5]. This can be done statically within a batch reactor, or continuously in a belt driven furnace. This is often a multistage process, requiring different temperatures and/or atmospheric conditions to remove thermally stable char residues in order to reclaim contaminant free fibres. The polymer decomposition is endothermic, and unlike oxidation (such as in the case of the fluidised bed), requires significant energy input. The sited energy input for pyrolysis recycling of composite materials varies throughout the literature. Energy-related inventory data obtained from a commercial operation from ELG Carbon Fibre (reproduced [5]) was used in this study, which is presented in Table S27.

It is assumed that all products from the polymer pyrolysis are eventually fully oxidised prior to releasing to the environment. Future state of pyrolysis technology may enable the condensation, collection and reprocessing of pyrolysis oils/waxes to produce feedstocks for the chemical industry, however, this has yet to be demonstrated for the thermoset polymers used in WTB structures. As such, the reclamation of the

polymeric fractions of the WTB waste has been omitted for pyrolysis recycling in this study. Fibre recovery rate is assumed to be 95%, with “waste fibres” assumed to be landfilled.

It is assumed that recycled glass, carbon and basalt fibre can offset the production of virgin glass, carbon and basalt fibre respectively. Due to exposure to high temperature during processing, strength loss is observed for glass and carbon fibres recovered using pyrolysis, therefore an offset knockdown factor has been applied to which dictates the replacement rate of virgin fibre counterparts.

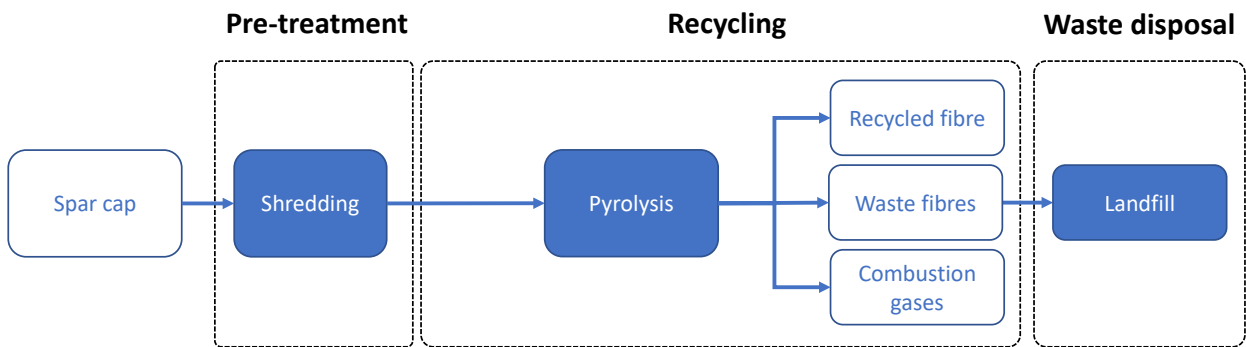


Figure S8 Process flow for WTB spar cap recycling using pyrolysis process.

Table S27 Energy input during pyrolysis recycling

Stage	Process	Energy	Energy source
Recycling	Pyrolysis	13.2 MJ/kg WTB [5]	Natural gas
		7.6 MJ/kg WTB [5]	UK mains electricity

10.9 Oxidation and calorific properties of material systems

The composition of gas produced during oxidation of blade materials (epoxy, PET, PU, carbon fibre, natural fibre) was estimated using stoichiometry, assuming all materials are fully oxidised to CO₂, NO₂ and H₂O. This data is used as input for end-of-life strategies which involve thermal decomposition of the WTB waste (EfW, cement kiln, pyrolysis). The relative mass of combustion gas products is presented in Table S28, it is assumed that glass and basalt fibre does not undergo oxidation and therefore has no combustion gases. The combustion gases from petroleum coke combustion (used as fuel in cement kiln) are provided by the UK Government which is reproduced in Table S28 [21].

Table S28 Chemical composition, combustion products and calorific value of various materials used in LCA

Material	Constituents / formula	Weight fraction in material (% wt.)	Combustion gas product(s)				Calorific value (MJ/kg)
			NO ₂ (kg NO ₂ / kg material)	N ₂ O (kg N ₂ O / kg material)	CH ₄ (kg CH ₄ / kg material)	CO ₂ (kg CO ₂ / kg material)	
Epoxy	Bisphenol A diglycidyl ether / C ₂₁ H ₂₄ O ₄	87	0.070	0	0	2.70	31.7 [22]
	Isophorone Dianmine / C ₁₀ H ₂₂ N ₂	13					

PET (PET core)	PET / $C_{10}H_8O_4$	100	0	0	0	2.29	24.1 [22]
PU (surface coatings)	PU / $C_{17}H_{16}N_2O_4$	100	0.29	0	0	2.40	26.6 [23]
Carbon fibre	Carbon / C	100	0	0	0	3.67	30 [24]
Flax / Hemp	Cellulose / $C_6H_{10}O_5$	90	0	0	0	1.47	13.5 ("grass/straw") [21]
	Water / H_2O	10					
Petroleum coke [21]	-	100	0	2.41509E-05	0.000122143	3.38	34.0

Table S29 Aggregated calorific value of wind blade waste from each of the scenarios assessed.

Blade scenario	Aggregated blade calorific value (MJ/kg)
Baseline (1)	15.55
Flax (2.2)	18.60
Hemp (3.2)	18.59
Basalt (4.2)	13.41

10.10 Fibre knockdown factors

Fibre knockdown factors were calculated for fibres reclaimed from mechanical and pyrolysis recycling. Since property degradation is experienced in many cases during recycling, the resultant reclaimed fibres cannot replace virgin fibre like-for-like without producing lower performance composites. The knockdown factor approach described below aims to quantify impact of this recycled fibre property degradation on resulting relevant performance characteristics of composites reinforced with said fibres. The method calculates the required increase in fibre weight fraction needed for a composite made with recycled fibre to achieve the same mechanical performance as that made with virgin fibre. This is given in Equation S24 as a function of the ratio between the fibre weight fractions of composites made with virgin and recycled fibres. The knockdown factor is used as a proxy for virgin fibre replacement rate when using recycled fibres to offset virgin fibre production.

Equation S24: Fibre knockdown factor approach

$$\text{Fibre knockdown factor} = 1 - \frac{W_{vF}}{W_{rF}}$$

Where W_{rF} and W_{vF} are the fibre weight fractions of model composites made with recycled and virgin fibre respectively and which meet the condition that both composites have identical relevant selected mechanical performance characteristic. To achieve this, the performance of a model composite reinforced with virgin fibre is calculated, then, using the degraded fibre properties following recycling, the performance of a composite reinforced with recycled fibres is calculated. The fibre weight fraction is then increased until the same performance is achieved with recycled fibre composites as was found using virgin counterpart. Tensile strength was selected to evaluate fibre knockdown. The method used to calculate these for the model composites is described below. It was assumed that recycled fibres are to be used as reinforcement in secondary injection moulding compound.

Table S30 Composition of model composite used in fibre knockdown assessment.

Fibre application	Polymer type	Weight fraction in virgin model composite			Fibre length
		Fibre	Polymer	Filler	
Injection moulding compound	Polypropylene	30%	70%	0%	0.5 mm [25]

The extended Kelly-Tyson model describes the tensile strength of discontinuous fibre composites. According to the Kelly-Tyson model the composite strength can be expressed in Equation S25.

Equation S25: Tensile strength of discontinuous fibre composites according to Kelly-Tyson model

$$\sigma_{cu} = \eta_o \left(\sum_{L_i < L_c} \left(\frac{\tau L_i}{D_f} \right) v_i + \sum_{L_i > L_c} \left(\frac{2\tau L_c}{D_f} \right) \left(1 - \left(\frac{L_c}{2L_j} \right) \right) v_j \right) + \sigma_m (1 - v_f)$$

Table S31 Input data used to calculate composite tensile strength using recycled fibres.

Symbol	Definition		Value
τ	Interfacial shear strength	GF	vGF: 17 MPa [26] rGF: 10 MPa [26]
		CF	vCF: 30 MPa [27] rCF: 30 MPa
L_f	Fibre length in model composite		6 mm
L_c	Critical fibre length		$L_c = \frac{\sigma_{fu} D_f}{2\tau}$
L_i	Fibre length shorter than critical fibre length		All fibres supercritical, $L_i = 0$ $L_j = L_f$
L_j	Fibre length longer than critical fibre length		
v_i	Volume fraction of fibres with subcritical length		All fibres supercritical, $v_i = 0$ $v_j = v_f$
v_j	Volume fraction of fibres with supercritical length		
σ_m	Matrix tensile strength		33 MPa [28]
E_m	Matrix tensile modulus		3400 MPa [28]
D_f	Fibre diameter	GF	17 μm [8]
		CF	7 μm [8]
η_o	Fibre orientation factor		3D random, $\eta_o = 0.2$
σ_{fu}	Fibre tensile strength	Virgin	GF - 1995 MPa [8] CF - 4900 MPa [29]
		Mechanical	GF - 78% retention [9]
		Pyrolysis	GF - 52% retention [30] CF - 72% retention [31]

Table S32 gives the calculated fibre knockdown factors for each of the fibre types and recycling routes.

Table S32 Fibre knockdown factors calculated for each recycling routes.

Fibre type	Mechanical	Pyrolysis
Glass fibre / basalt fibre	49.6%	49.6%
Carbon fibre	/	0.0%

11 Assumptions in basalt fibre production LCI dataset

The cradle-to-gate GWP for continuous basalt fibre (CBF) was not available in GaBi Sphera or Ecoinvent 3. The only LCA data that are currently available in the scientific literature are related to construction applications [32][33][34], and the LCA results are usually reported in terms of Functional Unit or are presented normalized and are not reported also in terms of mass unit of CBF raw material. To overcome this, an LCI dataset for this material was prepared to enable the wind blade LCA to be conducted. This section described the assumptions made in generating the GWP dataset for CBF production.

Pavlović et al. [35] reported the LCI data sources used in their LCA study of BFRP bars. Table S34 reports the energy intensities of electricity and thermal energy from natural gas of 4 different generations of manufacturing processes of CBF.

Table S33 Energy consumption of the manufacturing process of CBF

	Electricity	Natural gas	Natural gas
	[kWh/kg]	[m ³ /kg]	[MJ/kg]
1st generation	2.1	1.4	51.8
2nd generation	1.9	1.3	48.1
3rd generation	1.1	0.65	24.05
4th generation	0.85	0.35	12.95

Table S34 Specification of fourth generation process line TE BCF 2500-3000

Basic specifications	Measurement unit	TE BCF 2500
The line manufacturer	tones/year	2500 - 3000
Number of unit for primary BCF production	pcs.	14
The number of dies in the bushing,	pcs.	400
Gas flow rate	m ³ /h	110
Gas flow rate to produce 1 ton of BCF	m ³ /ton	350
Power consumption (220/380, 50Hz)	kVA	260
Electricity consumption to produce 1 ton of BCF	kWh	800 - 850
Mode of operation, continuous, year-round	days/year	350

According to S. Osnos [36], the 4th generation of modular production line of CBF is the most energy efficient currently available, reaching a production cost equal or below to the E-glass fibre production. That patented technology is currently used in production lines located in various countries: Ukraine, Russia, China, and US.

Considering the actual geo-political situation, the two countries of Ukraine and Russia have not been considered in this LCA as a geographical area where a potential CBF supplier could be located. Potential CBF suppliers located in China have not been considered in this LCA, as the energy grid mix in China is still based on a significant percentage of energy from coal, causing therefore a significant impact on Global Warming. A hypothetical supplier located in US was therefore the option considered in this report. The Company "Basalt Engineering, LLC", located in Winchester (US), is a CBF manufacturer: the manufacture of CBF was therefore considered to occur in this location.

Concerning the basalt extraction process and the location of basalt quarries in US, according to the website "Minedat.org", most of the basalt quarries are located on the west side of the US, in States like California,

Nevada, Oregon, Arizona and New Mexico. For this LCA it has been assumed that the basalt rock has been extracted from a basalt quarry located in New Mexico, nearby Albuquerque. Transportation between the quarry and the manufacturing site in Winchester has been assumed done by articulated lorry up to Albuquerque, followed by transportation by train up to Washington DC, followed by a final transportation by articulated lorry up to Winchester. Road transportation routes and the related distances have been calculated through the use of Google Maps®, while train transportation route has been assessed using the US railway network information provided by Amtrak®.

Table S35 Distances between the basalt quarry and the CBF manufacturing site

Transportation	Departure	Arrival	Distance [km]
Articulated lorry	Basalt quarry	Albuquerque	106
Train	Albuquerque	Washington DC	3319
Articulated lorry	Washington DC	Winchester	121

Once CBF are manufactured, for their transportation in the UK it has been considered a road transportation by articulated lorry up to the near port of Baltimore (US), and then transported by a cargo container ship up to Avonmouth (UK). Sea route distance has been estimated through the use of the website classic.searoutes.com.

Table S36 summarizes the distances between the CBF manufacturing site and the UK.

Table S36 Distances between the CBF manufacturing site and the UK.

Transportation	Departure	Arrival	Distance [km]
Articulated lorry	Winchester	Baltimore port	190
Cargo vessel	Baltimore port	Avonmouth port	6100

Transportation distances and energy intensities values of CBF manufacture have been used as input parameters of a GaBi Plan model, represented in Figure S9. Each block shown in the GaBi Plan model represents an individual LCI sub-process, related to:

- Basalt rock mining extraction
- Truck/Rail/Container ship transportation
- Diesel mix/Heavy fuel oil production
- Electricity production
- Thermal energy from natural gas
- CBF manufacture

More detailed information on the individual LCI secondary datasets used in the GaBi Plan are reported in Table S37.

The Functional Unit is equal to the production of 1 kg of CBF raw material, and it is matching with Reference Flow that has been considered in the GaBi Plan.

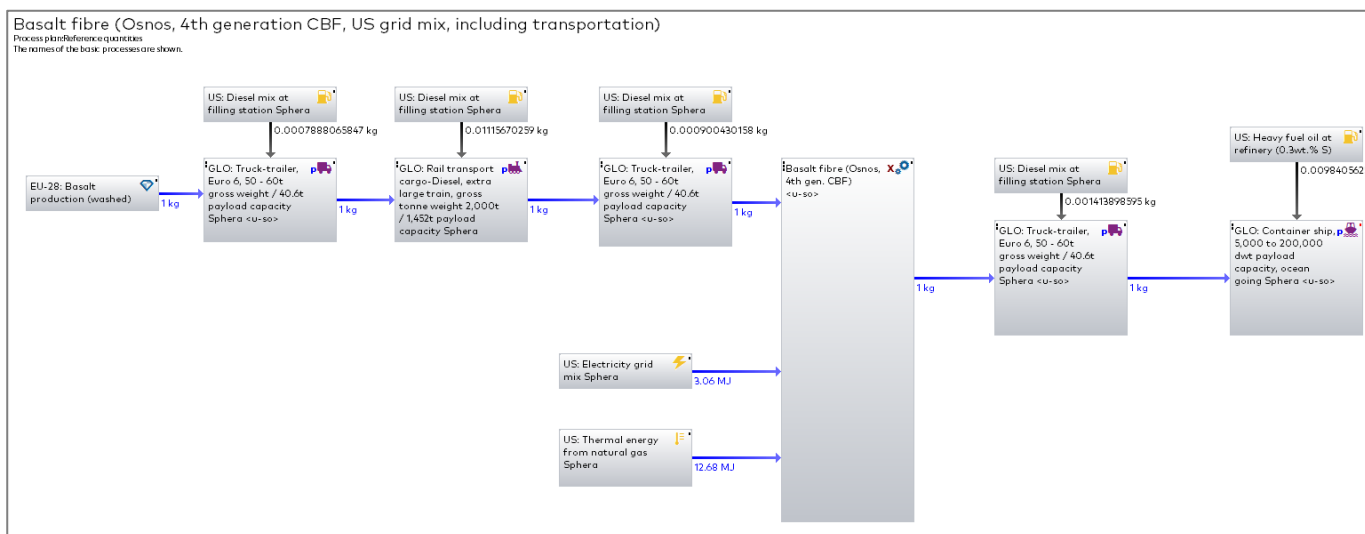


Figure S9 GaBi Plan model of CBF manufacture & transportation.

Table S37 LCI secondary datasets used in the GaBi model of CBF manufacture.

LCI dataset name	Geographical area	Source	Reference year
Basalt production (washed)	EU-28	Sphera	2021
Truck-trailer, Euro 6, 50 - 60t gross weight / 40.6t payload capacity	Global	Sphera	2021
Rail transport cargo-Diesel, extra large train, gross tonne weight 2,000t / 1,452t payload capacity	Global	Sphera	2021
Container ship, 5,000 to 200,000 dwt payload capacity, ocean going	Global	Sphera	2021
Diesel mix at filling station	US	Sphera	2018
Heavy fuel oil at refinery (0.3wt.% S)	US	Sphera	2018
Electricity grid mix	US	Sphera	2018
Thermal energy from natural gas	US	Sphera	2018
Basalt fibre (Osnos, 4th gen. CBF)	Global	Literature data [35][36]	2015

Table S38 reports the LCA results for the environmental impact categories used in the “CML 2001 – August 2016 update” Baseline method.

Table S38 LCA results related to the production of 1kg of CBF raw material.

Indicator	Total
CML2001 – Aug. 2016, Abiotic Depletion (ADP elements) [kg Sb eq.]	4.107E-07
CML2001 – Aug. 2016, Abiotic Depletion (ADP fossil) [MJ]	18.854
CML2001 – Aug. 2016, Acidification Potential (AP) [kg SO2 eq.]	2.166E-03
CML2001 – Aug. 2016, Eutrophication Potential (EP) [kg Phosphate eq.]	3.169E-04

CML2001 – Aug. 2016, Freshwater Aquatic Ecotoxicity Pot. (FAETP inf.) [kg DCB eq.]	1.997E-03
CML2001 – Aug. 2016, Global Warming Potential (GWP 100 years) [kg CO2 eq.]	1.356
CML2001 – Aug. 2016, Global Warming Potential (GWP 100 years), excl biogenic carbon [kg CO2 eq.]	1.355
CML2001 – Aug. 2016, Human Toxicity Potential (HTP inf.) [kg DCB eq.]	0.037
CML2001 – Aug. 2016, Marine Aquatic Ecotoxicity Pot. (MAETP inf.) [kg DCB eq.]	34.744
CML2001 – Aug. 2016, Ozone Layer Depletion Potential (ODP, steady state) [kg R11 eq.]	2.024E-12
CML2001 – Aug. 2016, Photochem. Ozone Creation Potential (POCP) [kg Ethene eq.]	1.856E-04
CML2001 – Aug. 2016, Terrestrial Ecotoxicity Potential (TETP inf.) [kg DCB eq.]	6.701E-04

12 Assumptions in PET foam production LCI dataset

Datasets for virgin PET foam (used as core materials in wind blade structures) was not available in GaBi Sphera or Ecoinvent 3. To overcome this, an LCI dataset for this material was prepared to enable the wind blade LCA to be conducted. This section described the assumptions made in generating the dataset for PET core production.

Production of polyethylene terephthalate (PET) foams can occur through many methods, and one of the most used is trough reactive extrusion [37]. This process is based on the reaction between PET and an appropriate blowing agent. The next step is the creation of foam by closing gas cells in the polymer matrix. Reactive processing of PET in order to extend macromolecular chains is undertaken at the polymer's melting point using in the same equipment as is used during the melting process. Chain extenders agents like pyromellitic dianhydride or epoxy compounds are commonly used for producing PET foams.

In this LCA, which has the goal to assess the environmental impact of manufacturing 1kg of PET foam, it has been considered the use of an epoxy resin compound. According to D. Misiura et al. [37] it is efficient in a proportion of 0.43%.

In order that the foaming process could occur it is necessary the use also a foaming agent, which might be in a solid, liquid, or gaseous form. According to D. Misiura et al. [37], the agents most often used in PET foaming are chemical compounds like hydrocerol CT534 or carbon dioxide used under high pressure. In this LCA carbon dioxide has been considered as a foaming agent, because its use is widely used, it has environmentally friendly properties and it presents high solubility in the polymer.

Considering the raw material densities listed in Table S39 and considering the percentage of epoxy resin compound of 0.43%, it has been calculated the amount of PET granulate, epoxy resin and carbon dioxide that are needed in input in order to produce 1kg of PET foam. These mass flows have been reported in the Life Cycle Inventory (LCI) input-output Table S40. It has also assumed that 10% of carbon dioxide is lost during the foaming process. The energy intensity of the foaming process has been considered similar to the same of an injection moulding process and sourced from the GaBi database, as also in this case the polymer needs to reach the melting point.

Table S39 – Raw materials densities.

Raw material	Density [kg/m ³]
PET granulate	1370
CO ₂ (@ 1atm 25° C)	1.145
Epoxy resin	1100

Table S40 – LCI input-output table to produce 1 kg of PET foam.

	Flow	Quantity	Amount	Units
INPUT	PET granulate	Mass	0.989	kg
	CO ₂	Mass	6.957E-03	kg
	Epoxy resin	Mass	4.255E-03	kg
	Electricity	Energy	2.222	kWh
OUTPUT	PET foam	Mass	1	kg
	CO ₂	Mass	6.325E-04	kg

Table S41 contains information about geographical area, source and reference year of the individual LCI secondary datasets that have been used in this LCA.

Table S41 – LCI secondary datasets used in the GaBi model of PET foam manufacture.

LCI dataset name	Geographical area	Source	Reference year
Polyethylene terephthalate bottle grade granulate (PET) via PTA	EU-28	Sphera	2021
Carbon dioxide by-product ethylene oxide (EO) via O2/methane	DE	Sphera	2021
Epoxy Resin (EP)	DE	Sphera	2021
Electricity grid mix	GB	Sphera	2021
PET foaming (density 160 kg/m3)	Global	Literature data [37]	2018

In Figure S10 is reported the GaBi Plan related to the manufacturing of 1kg of PET foam.

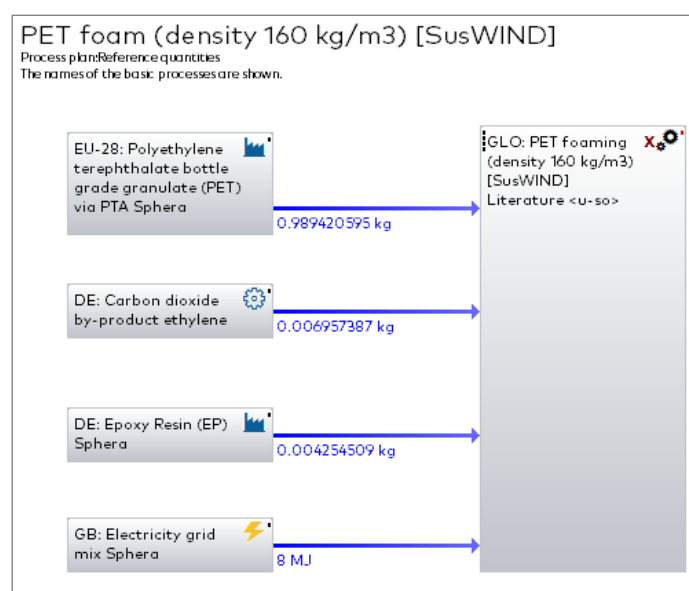


Figure S10 – GaBi Plan for the production of 1kg of PET foam.

The LCA results that comes from the Life Cycle Impact Assessment are reported in Table S42.

Table S42 - LCA results related to the production of 1kg of virgin PET foam.

Indicator	Total
CML2001 – Aug. 2016, Abiotic Depletion (ADP elements) [kg Sb eq.]	8.971E-07
CML2001 – Aug. 2016, Abiotic Depletion (ADP fossil) [MJ]	85.325
CML2001 – Aug. 2016, Acidification Potential (AP) [kg SO2 eq.]	4.859E-03
CML2001 – Aug. 2016, Eutrophication Potential (EP) [kg Phosphate eq.]	5.908E-04
CML2001 – Aug. 2016, Freshwater Aquatic Ecotoxicity Pot. (FAETP inf.) [kg DCB eq.]	1.775E-02

CML2001 – Aug. 2016, Global Warming Potential (GWP 100 years) [kg CO2 eq.]	3.530
CML2001 – Aug. 2016, Global Warming Potential (GWP 100 years), excl biogenic carbon [kg CO2 eq.]	3.528
CML2001 – Aug. 2016, Human Toxicity Potential (HTP inf.) [kg DCB eq.]	1.308E-01
CML2001 – Aug. 2016, Marine Aquatic Ecotoxicity Pot. (MAETP inf.) [kg DCB eq.]	197.231
CML2001 – Aug. 2016, Ozone Layer Depletion Potential (ODP, steady state) [kg R11 eq.]	4.198E-14
CML2001 – Aug. 2016, Photochem. Ozone Creation Potential (POCP) [kg Ethene eq.]	6.463E-04
CML2001 – Aug. 2016, Terrestrial Ecotoxicity Potential (TETP inf.) [kg DCB eq.]	6.936E-03
Primary energy demand from ren. And non ren. Resources (gross cal. Value) [MJ]	111.058
Primary energy demand from ren. And non ren. Resources (net cal. Value) [MJ]	103.402
Primary energy from non renewable resources (gross cal. Value) [MJ]	100.262
Primary energy from non renewable resources (net cal. Value) [MJ]	92.607
Primary energy from renewable resources (gross cal. Value) [MJ]	10.795
Primary energy from renewable resources (net cal. Value) [MJ]	10.795

13 LCI datasets

Table S43 LCI datasets used from Gabi Sphera

Material	Nation	Name	Source	GUID
Glass fibre	EU-28	Glass fibres	ts	{894AB0C2-A408-4824-8983-F886248F65BB}
Carbon fibre	GLO	Carbon fiber (CF; PAN-based; HT) - 01	Fraunhofer	{AA2BD1E0-7797-480B-88C4-82E56ED454E5}
Surface filler	EU-28	2-component PUR adhesive based on polyether and castor oil (approximation)	Sphera	{F17F4B67-08BD-485C-AFFC-ADF347E0D65B}
Gel coat	DE	Reactive resins based on polyurethane, unfilled/solventfree, polyol-free - DBC/IVK/VdL (A1-A3)	Sphera-EPD	{549EF33D-4107-46EF-BEC8-957C8B664BC2}
Primer	DE	Base coat/primer water-based (windows, white) (EN15804 A1-A3)	Sphera	{D69CBF67-A418-4C4D-860F-94DD82CC369E}
Top coat	EU-28	Top coat water-based (windows, white) (EN15804 A1-A3)	Sphera	{CA8A19AE-3429-47D5-9BAD-197149D9A413}
Adhesive	EU-28	Simple 2-component epoxy adhesive (approximation)	Sphera	{326d32e2-3478-41a7-984e-39236c0fe8ec}
Steel (bushings)	EU-28	Steel pipe (EN15804 A1-A3)	Sphera	{35599B72-6FE6-46D1-9F04-946F1D191AA9}
Aluminium (LSP)	EU-28	Aluminium foil	Sphera	{8DD54976-0163-4D6E-9FE4-FA09F72545ED}
Tackifier adhesive	EU-28	PVAc adhesive (approximation)	Sphera	{EA2CCC46-400B-4587-BC94-E42141AFCBCF}
Flow medium (infusion mesh)	EU-28	Polypropylene fibers (PP)	Sphera	{DB00901B-338F-11DD-BD11-0800200C9A66}

Landfill (plastic)	EU-28	Plastic waste on landfill	Sphera	{64197300-3307-11DD-BD11-0800200C9A66}
Landfill (glass)	EU-28	Inert matter (Glass) on landfill	Sphera	{ED41D893-EDCD-4B2A-B5E4-E1A992A8A04A}
Landfill (wood)	EU-28	Untreated wood on landfill	Sphera	{64197302-3307-11DD-BD11-0800200C9A66}
Electric energy	GB	Electricity grid mix	Sphera	{00043BD2-4563-4D73-8DF8-B84B5D8902FC}
Articulated lorry transport incl. fuel, Euro 0-6 mix, 40 t total weight, 27 t max payload	EU-28	Articulated lorry transport incl. fuel, Euro 0-6 mix, 40 t total weight, 27 t max payload	Sphera	{B444F4D1-3393-11DD-BD11-0800200C9A66}
Lorry transport incl. fuel, Euro 0-6 mix, 22 t total weight, 17.3t max payload	EU-28	Lorry transport incl. fuel, Euro 0-6 mix, 22 t total weight, 17.3t max payload	Sphera	{B444F4D3-3393-11DD-BD11-0800200C9A66}
Small lorry transport incl. fuel, Euro 0-6 mix, 7.5 t total weight, 3.3 t max payload	EU-28	Small lorry transport incl. fuel, Euro 0-6 mix, 7.5 t total weight, 3.3 t max payload	Sphera	{B4451BE0-3393-11DD-BD11-0800200C9A66}
Light fuel oil at refinery	GB	Light fuel oil at refinery	Sphera	{71D08EEF-D96C-4AC0-9AF9-10D86E2F8316}
Thermal energy from natural gas	GB	Thermal energy from natural gas	Sphera	{9006A870-750C-49B1-90B1-BC48372B88CA}
Flax fibre	FR	Flax long fibre	Sphera	{F0E27392-C4A2-4593-8603-C9F2A5274F9E}
Hemp fibre	DE	Hemp long fibre	Sphera	{3FBC0B5F-1455-403A-9F7B-F624EBC2C912}
Amine hardener	GB	Ethyleneamines (EDA, DETA, TETA, TEPA, PEHA)	Sphera	{32449A6A-E517-4EF9-A5B7-C0826A166878}
Epoxy resin	DE	Epoxy Resin (EP)	Sphera	{30DF02E7-D183-4EBA-987E-351AE4E42455}
Al ₂ O ₃	EU-28	Alumina production 2015	IAI	{C40A16BB-ED5F-42F2-9ED0-4D51B81BF95E}

SiO ₂	DE	Silica sand (Excavation and processing)	Sphera	{4CB83C4D-5A3E- 460D-9969- 9C42AD57C1FE}
CaO	EU-28	Lime (CaO; quicklime lumpy) (EN15804 A1-A3)	Sphera	{1598E3EA-812D- 4250-82FF- C477A7E57CFD}
Calcium carbonate	EU-28	Calcium carbonate > 63 microns IMA- Europe/ELCD	Sphera	{6006D87E-CCEE- 42B1-B203- F67C7C0BAD97}
Petroleum coke	EU-28	Petroleum coke at refinery	Sphera	{C9C86346-B056- 484B-BD6B- CD4B9266BA36}

14 Grade-to-Gate LCA raw data

Table S44. Cradle-to-gate LCA results for the various blade designs

	Blade scenario			
	Baseline (1)	Flax (2.2)	Hemp (3.2)	Basalt (4.2)
Impact Indicator	Impact per Reference Flow			
CML2001 - Aug. 2016, Abiotic Depletion (ADP elements) [kg Sb eq.]	2.119E-03	1.426E-03	1.425E-03	3.734E-04
CML2001 - Aug. 2016, Abiotic Depletion (ADP fossil) [MJ]	4.715E+03	4.613E+03	4.555E+03	4.347E+03
CML2001 - Aug. 2016, Acidification Potential (AP) [kg SO ₂ eq.]	5.981E-01	5.369E-01	5.309E-01	4.192E-01
CML2001 - Aug. 2016, Eutrophication Potential (EP) [kg Phosphate eq.]	7.563E-02	8.657E-02	7.858E-02	6.320E-02
CML2001 - Aug. 2016, Freshwater Aquatic Ecotoxicity Pot. (FAETP inf.) [kg DCB eq.]	9.244E-01	1.141E+00	9.915E-01	8.732E-01
CML2001 - Aug. 2016, Global Warming Potential (GWP 100 years) [kg CO ₂ eq.]	2.772E+02	2.618E+02	2.584E+02	2.552E+02
CML2001 - Aug. 2016, Global Warming Potential (GWP 100 years), excl biogenic carbon [kg CO ₂ eq.]	2.762E+02	2.693E+02	2.660E+02	2.541E+02
CML2001 - Aug. 2016, Human Toxicity Potential (HTP inf.) [kg DCB eq.]	1.253E+01	1.234E+01	1.227E+01	1.141E+01
CML2001 - Aug. 2016, Marine Aquatic Ecotoxicity Pot. (MAETP inf.) [kg DCB eq.]	2.019E+04	1.982E+04	1.956E+04	1.800E+04
CML2001 - Aug. 2016, Marine Aquatic Ecotoxicity Pot. (MAETP inf.) [kg DCB eq.]	2.019E+04	1.982E+04	1.956E+04	1.800E+04
CML2001 - Aug. 2016, Ozone Layer Depletion Potential (ODP, steady state) [kg R11 eq.]	6.322E-04	3.954E-04	3.924E-04	1.722E-09
CML2001 - Aug. 2016, Photochem. Ozone Creation Potential (POCP) [kg Ethene eq.]	5.185E-02	4.832E-02	4.766E-02	3.699E-02
CML2001 - Aug. 2016, Terrestrial Ecotoxicity Potential (TETP inf.) [kg DCB eq.]	1.138E+00	1.148E+00	1.148E+00	1.148E+00

15 Grade-to-Grave LCA raw data

Table S45 Cradle-to-grave LCA results for Baseline (1)

Blade scenario	Baseline (1)			
EoL scenario	Landfill	EfW	Cement kiln	Mechanical
Impact Indicator	Impact per Reference Flow			
CML2001 - Aug. 2016, Abiotic Depletion (ADP elements) [kg Sb eq.]	0.00212137 1	0.00211734 7	0.00200037 1	0.00155540 8
CML2001 - Aug. 2016, Abiotic Depletion (ADP fossil) [MJ]	5486.90410 3	5328.53726 6	3243.18688 8	3456.63532 5
CML2001 - Aug. 2016, Acidification Potential (AP) [kg SO2 eq.]	0.83589056 2	1.17377854 6	0.93068461 1	0.62156278 4
CML2001 - Aug. 2016, Eutrophication Potential (EP) [kg Phosphate eq.]	0.09154971 8	0.18116610 5	0.14684664 2	0.07665921 1
CML2001 - Aug. 2016, Freshwater Aquatic Ecotoxicity Pot. (FAETP inf.) [kg DCB eq.]	1.00401264 9	0.97917550 6	0.63281657 6	0.70940996 7
CML2001 - Aug. 2016, Global Warming Potential (GWP 100 years) [kg CO2 eq.]	373.614299 3	414.471016 5	249.802989 5	254.128911 6
CML2001 - Aug. 2016, Global Warming Potential (GWP 100 years), excl biogenic carbon [kg CO2 eq.]	323.806212 6	364.045478	199.361981 6	204.262427 1
CML2001 - Aug. 2016, Human Toxicity Potential (HTP inf.) [kg DCB eq.]	13.4071428 8	13.7982439 4	8.99150483 8	8.36573572 3
CML2001 - Aug. 2016, Marine Aquatic Ecotoxicity Pot. (MAETP inf.) [kg DCB eq.]	21338.0842 8	19767.7985 2	12320.0361 2	12453.2972
CML2001 - Aug. 2016, Marine Aquatic Ecotoxicity Pot. (MAETP inf.) [kg DCB eq.]	21338.0842 8	19767.7985 2	12320.0361 2	12453.2972
CML2001 - Aug. 2016, Ozone Layer Depletion Potential (ODP, steady state) [kg R11 eq.]	0.00063220 8	0.00063220 8	0.00063220 8	0.00063217 9
CML2001 - Aug. 2016, Photochem. Ozone Creation Potential (POCP) [kg Ethene eq.]	0.08078898	0.09924581 6	0.07392179 9	0.05804161 7
CML2001 - Aug. 2016, Terrestrial Ecotoxicity Potential (TETP inf.) [kg DCB eq.]	1.18364846 3	1.13913093 8	1.02594084 3	1.05097625 8

Table S46 Cradle-to-grave LCA results for Flax (2.2)

Blade scenario	Flax (2.2)			
EoL scenario	Landfill	EfW	Cement kiln	Mechanical
Impact Indicator	Impact per Reference Flow			
CML2001 - Aug. 2016, Abiotic Depletion (ADP elements) [kg Sb eq.]	0.001428 69	0.001423 92	0.001309	0.00106 4
CML2001 - Aug. 2016, Abiotic Depletion (ADP fossil) [MJ]	5389.077 27	5199.318 5	3110.698	3448.27 1
CML2001 - Aug. 2016, Acidification Potential (AP) [kg SO2 eq.]	0.775685 76	1.130034 63	0.895113	0.58955 8
CML2001 - Aug. 2016, Eutrophication Potential (EP) [kg Phosphate eq.]	0.103342 04	0.197506 63	0.164143	0.08897 1
CML2001 - Aug. 2016, Freshwater Aquatic Ecotoxicity Pot. (FAETP inf.) [kg DCB eq.]	1.221129 07	1.191469 62	0.825392	0.93626 2
CML2001 - Aug. 2016, Global Warming Potential (GWP 100 years) [kg CO2 eq.]	367.1537 01	407.0451 43	237.6768	244.929 2
CML2001 - Aug. 2016, Global Warming Potential (GWP 100 years), excl biogenic carbon [kg CO2 eq.]	323.3692 72	356.6473 96	188.37	203.478 3
CML2001 - Aug. 2016, Human Toxicity Potential (HTP inf.) [kg DCB eq.]	13.22328 81	13.57429 88	8.858417	8.38361 6
CML2001 - Aug. 2016, Marine Aquatic Ecotoxicity Pot. (MAETP inf.) [kg DCB eq.]	20980.38 75	19117.71 98	12072.2	12449.7 9
CML2001 - Aug. 2016, Marine Aquatic Ecotoxicity Pot. (MAETP inf.) [kg DCB eq.]	20980.38 75	19117.71 98	12072.2	12449.7 9
CML2001 - Aug. 2016, Ozone Layer Depletion Potential (ODP, steady state) [kg R11 eq.]	0.000395 42	0.000395 42	0.000395	0.00039 5
CML2001 - Aug. 2016, Photochem. Ozone Creation Potential (POCP) [kg Ethene eq.]	0.079381 73	0.096899 5	0.072188	0.05693 1
CML2001 - Aug. 2016, Terrestrial Ecotoxicity Potential (TETP inf.) [kg DCB eq.]	1.196340 26	1.143681 91	1.038681	1.06996 8

Table S47 Cradle-to-grave LCA results for Hemp (3.2)

Blade scenario	Hemp (3.2)			
EoL scenario	Landfill	EfW	Cement kiln	Mechanical
Impact Indicator	Impact per Reference Flow			
CML2001 - Aug. 2016, Abiotic Depletion (ADP elements) [kg Sb eq.]	0.001427	0.001422	0.001308	0.001065
CML2001 - Aug. 2016, Abiotic Depletion (ADP fossil) [MJ]	5330.765	5142.811	3090.502	3426.005
CML2001 - Aug. 2016, Acidification Potential (AP) [kg SO2 eq.]	0.769737	1.121038	0.890419	0.587138
CML2001 - Aug. 2016, Eutrophication Potential (EP) [kg Phosphate eq.]	0.095315	0.188668	0.155928	0.081309
CML2001 - Aug. 2016, Freshwater Aquatic Ecotoxicity Pot. (FAETP inf.) [kg DCB eq.]	1.071392	1.042019	0.681329	0.791493
CML2001 - Aug. 2016, Global Warming Potential (GWP 100 years) [kg CO2 eq.]	363.7707	403.1637	236.491	243.697
CML2001 - Aug. 2016, Global Warming Potential (GWP 100 years), excl biogenic carbon [kg CO2 eq.]	320.0758	352.8548	187.2732	202.3362
CML2001 - Aug. 2016, Human Toxicity Potential (HTP inf.) [kg DCB eq.]	13.15624	13.5047	8.875192	8.404172
CML2001 - Aug. 2016, Marine Aquatic Ecotoxicity Pot. (MAETP inf.) [kg DCB eq.]	20721.75	18876.85	11975.29	12350.78
CML2001 - Aug. 2016, Marine Aquatic Ecotoxicity Pot. (MAETP inf.) [kg DCB eq.]	20721.75	18876.85	11975.29	12350.78
CML2001 - Aug. 2016, Ozone Layer Depletion Potential (ODP, steady state) [kg R11 eq.]	0.000392	0.000392	0.000392	0.000392
CML2001 - Aug. 2016, Photochem. Ozone Creation Potential (POCP) [kg Ethene eq.]	0.078735	0.096085	0.071797	0.056656
CML2001 - Aug. 2016, Terrestrial Ecotoxicity Potential (TETP inf.) [kg DCB eq.]	1.195243	1.143091	1.039777	1.070867

Table S48 Cradle-to-grave LCA results for Basalt (4.2)

Blade scenario	Basalt (4.2)			
EoL scenario	Landfill	EfW	Cement kiln	Mechanical
Impact Indicator	Impact per Reference Flow			
CML2001 - Aug. 2016, Abiotic Depletion (ADP elements) [kg Sb eq.]	0.000376	0.000371	0.000358	0.000358
CML2001 - Aug. 2016, Abiotic Depletion (ADP fossil) [MJ]	5119.691	4953.911	3519.238	3804.297
CML2001 - Aug. 2016, Acidification Potential (AP) [kg SO2 eq.]	0.657141	1.052413	0.899106	0.618742
CML2001 - Aug. 2016, Eutrophication Potential (EP) [kg Phosphate eq.]	0.079115	0.184003	0.160563	0.086195
CML2001 - Aug. 2016, Freshwater Aquatic Ecotoxicity Pot. (FAETP inf.) [kg DCB eq.]	0.952613	0.926168	0.652644	0.738623
CML2001 - Aug. 2016, Global Warming Potential (GWP 100 years) [kg CO2 eq.]	351.5933	391.6247	271.0451	279.6102
CML2001 - Aug. 2016, Global Warming Potential (GWP 100 years), excl biogenic carbon [kg CO2 eq.]	301.6697	341.0711	220.4965	229.6563
CML2001 - Aug. 2016, Human Toxicity Potential (HTP inf.) [kg DCB eq.]	12.29302	12.79977	9.555471	8.974547
CML2001 - Aug. 2016, Marine Aquatic Ecotoxicity Pot. (MAETP inf.) [kg DCB eq.]	19178.07	17498.19	13159.67	13495.83
CML2001 - Aug. 2016, Marine Aquatic Ecotoxicity Pot. (MAETP inf.) [kg DCB eq.]	19178.07	17498.19	13159.67	13495.83
CML2001 - Aug. 2016, Ozone Layer Depletion Potential (ODP, steady state) [kg R11 eq.]	1.72E-09	1.72E-09	1.7E-09	-2.9E-08
CML2001 - Aug. 2016, Photochem. Ozone Creation Potential (POCP) [kg Ethene eq.]	0.066233	0.087697	0.071179	0.056673
CML2001 - Aug. 2016, Terrestrial Ecotoxicity Potential (TETP inf.) [kg DCB eq.]	1.197309	1.142788	1.06571	1.10322

16 References

1. Bortolotti, P.; Berry, D.; Murray, R.; Gaertner, E.; Jenne, D.; Damiani, R.; Barter, G.; Dykes, K. A Detailed Wind Turbine Blade Cost Model. 2019. Available online: <https://www.nrel.gov/docs/fy19osti/73585.pdf> (accessed on 23 April 2024).
2. Jalili, S.; Maheri, A.; Ivanovic, A. Cost Modelling for Offshore Wind Farm Decommissioning. 2022. Available online: https://northsearegion.eu/media/19936/cost-modelling_final_2022.pdf (accessed on 23 April 2024).
3. SPARTA. System Performance, Availability and Reliability Trend Analysis: Portfolio Review 2016. No. March, 2017. Available online: https://s3-eu-west-1.amazonaws.com/media.ore.catapult/wp-content/uploads/2017/03/28102600/SPARTAbrochure_20March-1.pdf (accessed on 23 April 2024).
4. Palmer, J.; Ghita, O.R.; Savage, L.; Evans, K.E. Successful closed-loop recycling of thermoset composites. *Compos. Part A Appl. Sci. Manuf.* **2009**, *40*, 490–498. <https://doi.org/10.1016/j.compositesa.2009.02.002>.
5. Meng, F.; Olivetti, E.A.; Zhao, Y.; Chang, J.C.; Pickering, S.J.; McKechnie, J. Comparing Life Cycle Energy and Global Warming Potential of Carbon Fiber Composite Recycling Technologies and Waste Management Options. *ACS Sustain. Chem. Eng.* **2018**, *6*, 9854–9865. <https://doi.org/10.1021/acssuschemeng.8b01026>.
6. AOC Trusted Solutions. Renewable Value: Recycling Guide. 2020. Available online: <https://aocresins.com/en-emea/downloads/renewable-value-composites-recycling/#> (accessed on 23 April 2024).
7. Shuaib, N.A.; Mativenga, P.T. Energy demand in mechanical recycling of glass fibre reinforced thermoset plastic composites. *J. Clean. Prod.* **2016**, *120*, 198–206. <https://doi.org/10.1016/j.jclepro.2016.01.070>.
8. Barbero, E.J. *Introduction to Composite Materials Design*; CRC Press: Boca Raton, FL, USA, 1998.
9. Palmer, J.A.T. *Mechanical Recycling of Automotive Composites for Use as Reinforcement in Thermoset Composites*; University of Exeter: Exeter, UK, 2009.
10. Chartered Institution of Building Services Engineers (CIBSE), “TM46: 2008 Energy benchmarks CIBSE,” London, 2008.
11. M. J. Kaiser and B. Snyder, “Offshore Wind Energy Cost Modeling: Installation and Decommissioning,” in *Green Energy and Technology*, Springer, 2014.
12. Y. Dalgic, I. Lazakis, O. Turan, and S. Judah, “Investigation of Optimum Jack-Up Vessel Chartering Strategy for Offshore Wind Farm O&M Activities,” *Ocean Eng.*, vol. 95, pp. 106–115, 2014, doi: 10.1016/j.oceaneng.2014.12.011.
13. G.L. Garrad Hassan, “A Guide to UK Offshore Wind Operations and Maintenance,” 2013. doi: 10.13140/RG.2.2.12957.36328.
14. Offshore Renewable Energy Catapult, “Decarbonising Marine Operation North Sea Offshore Wind: Innovation Roadmap produced for the UK Government DfT and FCDO,” 2021. [Online]. Available: <https://assets.publishing.service.gov.uk/media/60e5ce8ae90e0764c8f0a3d4/decarbonising-maritime-operations-in-north-sea-offshore-wind-o-and-m.pdf>.
15. S. Jalili, A. Maheri, and A. Ivanovic, “Cost and Emission Analyses of Decommissioning of Offshore Wind Farms Using Reverse Installation Method : Cases of Lincs Limited , Gunfleet Sands , and Horns Rev I Wind Farms,” 2022. [Online]. Available: <https://northsearegion.eu/media/21105/cost-and-emission-analysis-of-decommissioning-og-offshore-wind-farms-using-reverse-installation-method.pdf>.
16. A. Arvesen, C. Birkeland, and E. G. Hertwich, “The Importance of Ships and Spare Parts in LCAs of Offshore Wind Power,” *Environ. Sci. Technol.*, vol. 47, pp. 2948–2956, 2013, doi: 10.1021/es304509r.
17. F. Di Maria, S. Contini, G. Bidini, A. Boncompagni, M. Lasagni, and F. Sisani, “Energetic Efficiency of an Existing Waste to Energy Power Plant,” *Energy Procedia*, vol. 101, pp. 1175–1182, 2016, doi: 10.1016/j.egypro.2016.11.159.
18. Tolvik Consulting, “UK Energy from Waste Statistics – 2019,” 2019. [Online]. Available: <https://www.tolvik.com/published-reports/view/uk-energy-from-waste-statistics-2019/>.
19. A. M. Joseph, R. Snellings, P. Van den Heede, S. Matthys, and N. De Belie, “The use of municipal solidwaste incineration ash in various building materials: A Belgian point of view,” *Materials (Basel)*, vol. 11, p. 141, 2018, doi: 10.3390/ma11010141.

20. H. Mann, C. Roloff, T. Hagemeyer, D. Thévenin, and J. Tomas, "Model-based experimental data evaluation of separation efficiency of multistage coarse particle classification in a zigzag apparatus," *Powder Technol.*, vol. 313, pp. 145–160, 2017, doi: 10.1016/j.powtec.2017.03.003.
21. Department of Business Energy and Industrial Strategy, "2020 Government greenhouse gas conversion factors for company reporting: Methodology paper," 2020. [Online]. Available: <https://assets.publishing.service.gov.uk/media/5f119b673a6f405c059f6060/conversion-factors-2020-methodology.pdf>.
22. L. Costiuc, S. Patachia, L. Baltas, and M. Tieren, "Investigation on Energy Density of Plastic Waste Materials," in *The 26th International Conference on Solid Waste Technology and Management*, 2011, pp. 930–939.
23. H. Wang, Y. Tian, X. Chen, and J. Li, "Kinetic and Synergetic Effect Analysis of the Co-Combustion of Coal Blended with Polyurethane Materials," *ACS Omega*, vol. 5, pp. 26005–26014, 2020, doi: 10.1021/acsomega.0c03449.
24. H. Sukanto, W. W. Raharjo, D. Ariawan, and J. Triyono, "Carbon fibers recovery from CFRP recycling process and their usage: A review," *IOP Conf. Ser. Mater. Sci. Eng.*, vol. 1034, p. 012087, 2021, doi: 10.1088/1757-899x/1034/1/012087.
25. J. L. Thomason, "The influence of fibre length and concentration on the properties of glass fibre reinforced polypropylene: 5. Injection moulded long and short fibre PP," *Compos. Part A Appl. Sci. Manuf.*, vol. 33, no. 12, pp. 1641–1652, 2002, doi: [http://dx.doi.org/10.1016/S1359-835X\(02\)00179-3](http://dx.doi.org/10.1016/S1359-835X(02)00179-3).
26. L. Yang and J. L. Thomason, "Development and application of micromechanical techniques for characterising interfacial shear strength in fibre-thermoplastic composites," *Polym. Test.*, vol. 31, no. 7, pp. 895–903, 2012, doi: <https://doi.org/10.1016/j.polymertesting.2012.07.001>.
27. G. Cai, M. Wada, I. Ohsawa, S. Kitaoka, and J. Takahashi, "Interfacial adhesion of recycled carbon fibers to polypropylene resin: Effect of superheated steam on the surface chemical state of carbon fiber," *Compos. Part A Appl. Sci. Manuf.*, vol. 120, pp. 33–40, 2019, doi: 10.1016/j.compositesa.2019.02.020.
28. Resin Library Supplies, "Polyester Resin: Preparation, storage and usage of unsaturated polyester resin for glass fibre-based laminates." <https://www.resinlibrary.com/knowledge/article/polyester-resin/> (accessed Apr. 23, 2024).
29. E. Pakdel, S. Kashi, R. Varley, and X. Wang, "Recent progress in recycling carbon fibre reinforced composites and dry carbon fibre wastes," *Resour. Conserv. Recycl.*, vol. 166, p. 105340, 2021, doi: 10.1016/j.resconrec.2020.105340.
30. A. E. Krauklis, C. W. Karl, A. I. Gagani, and J. K. Jørgensen, "Composite Material Recycling Technology - State of the Art and Sustainable Development for the 2020s," *J. Compos. Sci.*, vol. 5, p. 28, Jan. 2021, doi: 10.3390/jcs5010028.
31. S. J. Pickering et al., "Developments in the fluidised bed process for fibre recovery from thermoset composites," 2015, [Online]. Available: https://www.researchgate.net/publication/301849557_Developments_in_the_fluidised_bed_process_for_fibre_recovery_from_thermoset_composites/link/5854164608ae77ec370458a2/download?_tp=eyJjb250ZXh0Ijp7ImZpcnN0UGFnZSI6InB1YmxpY2F0aW9uIiwicGFnZSI6InB1YmxpY2F0aW9u.
32. Y. Zhang, T. Huang, Y. Wang, J. Zhang, and J. Wang, "Environmental assessment of concrete beams strengthened with fibre-reinforced polymer," *Proc. Inst. Civ. Eng. Eng. Sustain.*, vol. 174, no. 1, pp. 37–45, 2020, doi: 10.1680/jensu.20.00011.
33. M. Inman, E. R. Thorhallsson, and K. Azrague, "A Mechanical and Environmental Assessment and Comparison of Basalt Fibre Reinforced Polymer (BFRP) Rebar and Steel Rebar in Concrete Beams," *Energy Procedia*, vol. 111, pp. 31–40, 2017, doi: 10.1016/j.egypro.2017.03.005.
34. K. Azrague, M. Rose Inman, L.-I. Alnaes, R. Dahl Schlanbusch, and B. Jóhannesson, "Life Cycle Assessment as a tool for resource optimisation of continuous basalt fibre production in Iceland," 2016. [Online]. Available: http://dc.engconfintl.org/lca_wastehttp://dc.engconfintl.org/lca_waste/10.
35. A. Pavlović, T. Donchev, D. Petkova, and N. Staletović, "Sustainability of alternative reinforcement for concrete structures: Life cycle assessment of basalt FRP bars," *Constr. Build. Mater.*, vol. 334, p. 127424, 2022, doi: 10.1016/j.conbuildmat.2022.127424.

36. S. Osnos, "Present and future of basalt fibre technology, manufacturing and market development," *JEC Composites Magazine*, vol. 53, pp. 15–18, Oct. 01, 2016.
37. D. Misiura and T. M. Majka, "An overview on obtaining foamed PET by reactive extrusion," *Czas. Tech.*, vol. 4, pp. 97–102, 2018, doi: 10.4467/2353737xct.18.057.8369.